NASA Technical Memorandum 4057

Flight-Management Strategies for Escape From Microburst Encounters

(NASA-TM-4057) FLIGHT-MANAGEMENT STRATEGIES FOR ESCAPE FROM MICROBURST ENCOUNTERS M.S. Thesis - George Washington Univ. (NASA) 29 p CSCL 01C

N88-25461

Unclas H1/08 0146802

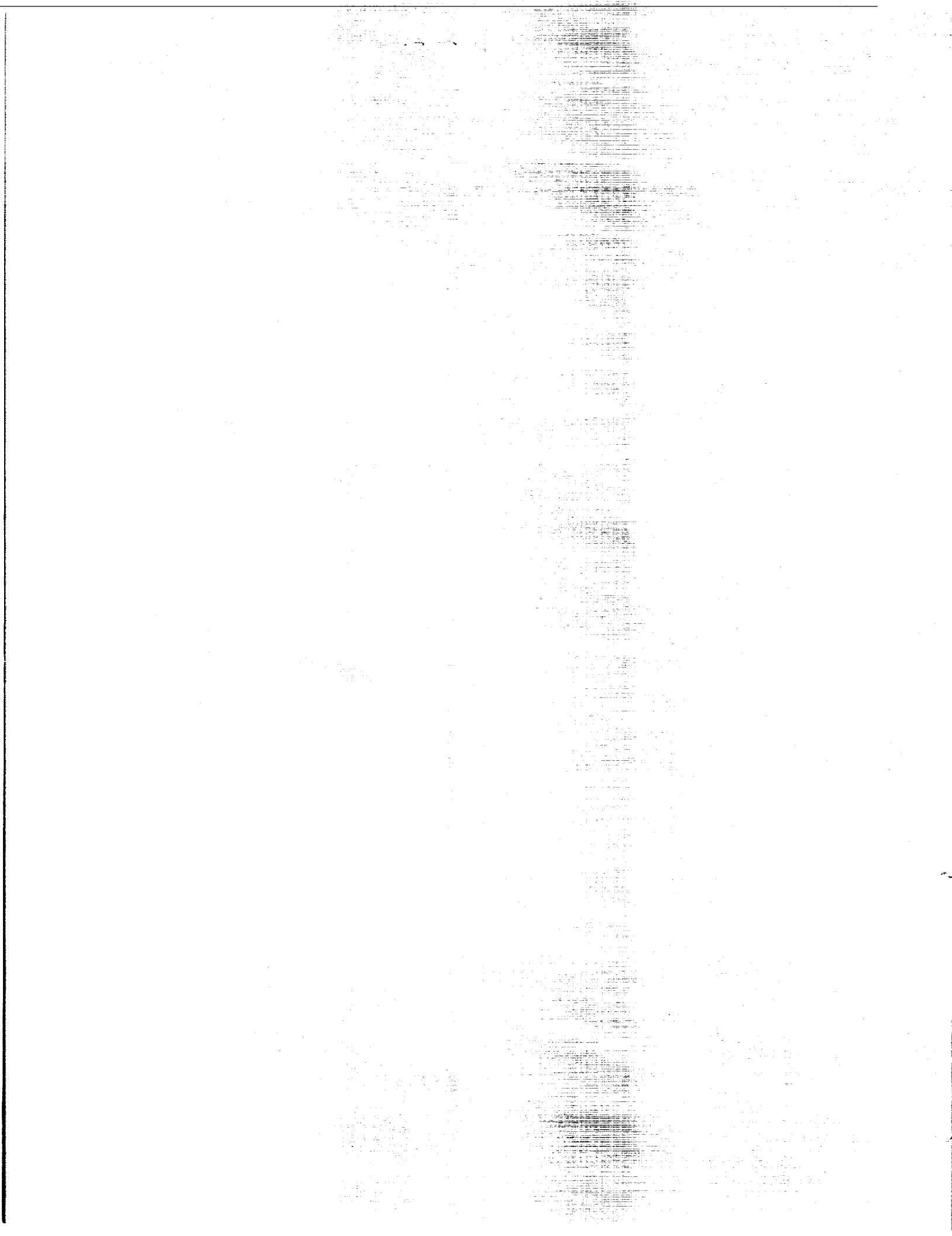

NASA Technical Memorandum 4057

Flight-Management Strategies for Escape From Microburst Encounters

David A. Hinton
Langley Research Center
Hampton, Virginia

National Aeronautics
and Space Administration

**Scientific and Technical
Information Division**

1988

Summary

An effort is in progress by the National Aeronautics and Space Administration (NASA), the Federal Aviation Administration (FAA), and industry to reduce the threat of convective microburst wind-shear phenomena to aircraft through hazard characterization, improved detection and warning, development of recovery flight techniques, and crew training. The goal of this study was to develop and test a candidate set of strategies for recovery from inadvertent microburst encounters during takeoff. The assumptions are made that the presence of the microburst is not known until the airplane enters it and that the structure and strength of the flow field ahead of the airplane are not known. Candidate strategies were developed and evaluated using a fast-time simulation consisting of a simple point-mass performance model of a transport-category airplane flying through a simple analytical microburst model.

The results of this study indicate that the characteristics of a recovery strategy that best utilize available airplane energy in a takeoff microburst encounter include an initial reduction in pitch attitude early in the encounter to reduce the climb rate, followed by an increase in pitch-up to the stick-shaker angle of attack. The stick-shaker angle of attack should be reached just as the airplane is exiting the microburst. The shallowest angle of climb necessary for obstacle clearance should be maintained. If the altitude is higher than necessary, an intentional descent to reduce the airspeed deceleration should be used. The rate of descent must be small and varied with altitude to prevent undershooting a given minimum altitude. Minimum altitudes reached during recoveries were, in general, very sensitive to small changes in microburst strength; 5-percent changes in shear strength produced an average of 60-percent change in recovery altitude. Of five strategies tested, two strategies based on flight-path angle stood out as having the highest recovery altitudes and the least sensitivity to variations in the encounter scenarios.

Introduction

Numerous air-carrier accidents and incidents have resulted from inadvertent encounters with the atmospheric wind shear associated with microburst phenomena; some of these accidents have resulted in heavy loss of life. A microburst is a strong, localized downdraft that strikes the ground, producing winds that diverge radially from the impact point. An airplane penetrating the center of a microburst initially encounters an increasing head wind, which improves airplane climb-angle performance, and then encounters a strong downdraft and a rapidly increasing tail wind. The effects of the downdraft and increasing tail wind may easily exceed the climb and acceleration capabilities of the airplane, which would cause an unavoidable loss of altitude and airspeed. These encounters have resulted from the fact that the microburst and its impact on airplane performance have been recognized for only a relatively short time (refs. 1 and 2), and from the fact that the ability to reliably predict or detect a microburst in an airplane's flight path, in an operational environment, does not yet exist. The physics of microburst winds have only recently been understood in detail, and recovery during inadvertent airplane encounters may require techniques that are unique to microbursts and counterintuitive to flight crews.

Previous research has been conducted on control strategies for maintaining a given flight path in the presence of strong wind shears (refs. 3 and 4). These studies have developed control laws to permit the airplane to track a predefined path, such as the glide slope of an instrument landing system. This tracking will be possible in many wind-shear encounters but will not be possible if the shear is severe. With currently available sensors, the severity of a shear cannot be known until the airplane has successfully flown through it. Other research (ref. 5) has shown the performance available from an airplane following an optimal trajectory when full knowledge of the microburst flow field is known. In that study, the emphasis was on escape from inadvertent microburst encounters, and the trajectory was a result of the optimization procedure, not an assumed goal. Later research by the same authors considered wind-shear recovery performance when only local wind knowledge is available (ref. 6), and considered the maneuvering required of the pilot (ref. 7).

This paper describes an effort aimed at developing techniques for flying "near-optimal" trajectories, during inadvertent microburst encounters, when the flow field ahead of the airplane is not known. Only the takeoff microburst encounter case is considered. Lessons learned from previous and ongoing research were used to develop five candidate microburst escape strategies. The characteristics of these strategies were then evaluated using a fast-time simulation consisting of a simple point-mass performance model of a transport airplane flying through a simple microburst model. Additional refinements to the candidate recovery procedures were then made. The sensitivity of the candidate recovery strategies to slight variations in microburst strength and encounter conditions was determined. The study was done in preparation for a planned piloted simulation study of microburst recovery guidance.

Symbols

Values are expressed in U.S. Customary Units. A dot above a symbol denotes a derivative with respect to time. The units presented were used in derivations and computer software. Units in common use in the aircraft industry were used in cockpit displays and for discussion in the text; these units are shown below in parentheses.

A	gradient of horizontal flow in axisymmetric shear, per sec
C_D	nondimensional drag coefficient
$C_{D,o}$	drag coefficient at zero angle of attack
C_L	nondimensional lift coefficient
$C_{L,o}$	lift coefficient at zero angle of attack
C_{L_α}	lift coefficient change with angle of attack, per rad
D	airplane total drag, lbf
E	airplane total energy, ft-lbf
Es	specific total energy (energy per unit weight), also called energy height, ft
F	"F-factor" measure of wind-shear impact on capability of airplane flight-path angle, rad
G	wind-shear term in acceleration strategy algorithm
g	gravitational acceleration, ft/sec^2
h	airplane altitude, ft
$\dot{h}_p$	airplane potential rate of climb, ft/sec (ft/min)
K	gain in flight-path-angle strategy law
KW	horizontal wind gain in microburst model
L	total airplane lift, lbf
m	airplane mass, slugs
q	dynamic pressure, lbf/ft^2
r	radial distance from stagnation point in axisymmetric downflow, ft
S	airplane wing area, ft^2
T	total engine thrust, lbf
t	time, sec
TEMP	a temporary value in computations
U	radial wind speed in axisymmetric downflow, ft/sec
V	airplane true airspeed, ft/sec (knots)
V_g	airplane ground speed, ft/sec (knots)
W	airplane weight, lbf
Wh	vertical wind speed, up positive, ft/sec (ft/min)
Wx	horizontal wind speed, tail wind positive, ft/sec (knots)
XL	width of horizontal wind gradient, ft
$X1$	starting point of horizontal wind gradient, ft
x	horizontal distance across ground, ft
z	height above flat plate in axisymmetric downflow, ft
α	wing angle of attack, rad (deg)
γ_a	flight-path angle with respect to air mass, rad
$\gamma_{a,p}$	potential flight-path angle with respect to air mass, rad
γ_i	inertial flight-path angle, rad
$\gamma_{i,p}$	inertial potential flight-path angle, rad
λ	gain in acceleration strategy
θ	airplane pitch attitude, rad (deg)

Energy Concepts

The concepts of airplane total energy and potential flight-path angle were used in the development of the guidance strategies and are useful in interpreting the results of the encounters. The airplane flight path and the wind components are related by the coordinate system shown in figure 1. The airplane total energy is defined as the sum of the air-mass relative kinetic energy and the inertial potential energy. Air-mass kinetic energy is used since only airspeed, not

ground speed, describes the ability of the airplane to climb or maintain altitude. Inertial potential energy is likewise used since it is altitude above the ground that is useful to the airplane. Airplane total energy is then defined as

$$E = 0.5mV^2 + mgh \tag{1}$$

where V is airspeed, m is airplane mass, and h is altitude. The specific total energy (E per unit weight), or energy height, is defined as

$$Es = \frac{V^2}{2g} + h \tag{2}$$

The rate of change of Es is also the potential rate of climb of the airplane, assuming a negligible energy loss when trading airspeed for climb rate, and is defined as

$$\dot{E}s = \dot{h}_p = V\left(\frac{\dot{V}}{g}\right) + \dot{h} \tag{3}$$

This quantity can be measured directly by existing total-energy sensors and displays (ref. 8).

The impact of wind shear on the energy state of the airplane and the ability of the airplane to climb in that shear can now be discussed. From the equations of motion developed in reference 5, the airspeed acceleration in the presence of shear can be written as follows:

$$\dot{V} = \frac{T}{m}\cos\ \alpha - \frac{D}{m} - g\ \sin\ \gamma_a - \dot{W}x\cos\ \gamma_a - \dot{W}h\sin\ \gamma_a \tag{4}$$

The term $\dot{W}h\ \sin\ \gamma_a$ is insignificant and can be dropped. Setting $\dot{V} = 0$ and rearranging terms gives the steady-state air-mass flight-path angle in the presence of a horizontal wind shear. The cosine of γ_a is very close to unity during a microburst encounter, and this approximation is made in the $\dot{W}x$ term to produce an analytical equation. No other small-angle approximations are necessary during the development of the energy equations. The potential air-mass climb angle can then be described as follows:

$$\gamma_{a,p} = \sin^{-1}\left(\frac{T\cos\ \alpha - D}{W} - \frac{\dot{W}x}{g}\right) \tag{5}$$

The inertial flight-path angle can be determined from air-mass flight-path angle as follows:

$$\gamma_i = \tan^{-1}\frac{V\sin\ \gamma_a + Wh}{V_g} \tag{6}$$

Substituting equation (5) into equation (6) produces the inertial potential flight-path angle as follows:

$$\gamma_{i,p} = \tan^{-1}\left(\frac{T\cos\ \alpha - D}{W} - \frac{\dot{W}x}{g}\left(\frac{V}{V_g}\right) + \frac{Wh}{V_g}\right) \tag{7}$$

The actual flight-path angle can be related to the potential flight-path angle by airspeed acceleration, because airspeed can be traded for climb gradient with essentially constant energy rates. From equation (3),

$$\dot{h} = \dot{h}_p - V\left(\frac{\dot{V}}{g}\right) \tag{8}$$

Flight-path angle is related to rate of climb by

$$\dot{h} = V_g \tan\ \gamma_i \tag{9a}$$

and

$$\dot{h}_p = V_g \tan\ \gamma_{i,p} \tag{9b}$$

Then

$$V_g \tan\ \gamma_i = V_g \tan\ \gamma_{i,p} - V\left(\frac{\dot{V}}{g}\right) \tag{10}$$

Combining equations (7) and (10) and rearranging terms produces the actual flight-path angle in the presence of wind shear and airspeed changes as follows:

$$\gamma_i = \tan^{-1}\left(\frac{T\cos\ \alpha - D}{W} - \frac{\dot{W}x}{g} + \frac{Wh}{V} - \frac{\dot{V}}{g}\right)\frac{V}{V_g} \tag{11}$$

The two wind terms describe the wind-shear impact on the climb-angle capability of the airplane, in terms of the horizontal shear and vertical winds, and are referred to as the "F-factor," where

$$F = \frac{\dot{W}x}{g} - \frac{Wh}{V} \tag{12}$$

By using small-angle approximations, equation (11) can be simplified. The equation can be further simplified by considering only the change in flight-path angle caused by the shear rate and ignoring the change in flight-path angle caused by the instantaneous wind speed. This is done by setting $V = V_g$. The resulting expression for flight-path angle is

$$\gamma_i = \frac{T - D}{W} - \frac{\dot{W}x}{g} + \frac{Wh}{V} - \frac{\dot{V}}{g} \tag{13}$$

Equations (11) and (13) describe the impact of the wind shear on flight path and the ability of the

airplane to compensate through airspeed deceleration. The airspeed margin above the stick-shaker airspeed can be used to continue a climb or to reduce a descent rate. Once the stick-shaker angle of attack is reached, no further deceleration is available for the recovery of climb performance. The flight-management problem can then be considered a question of how best to distribute the available reserve airspeed during a microburst encounter.

The effect of a horizontal wind shear on airplane performance is further illustrated by figure 2, which shows the steady-state climb performance of the modeled airplane as a function of airspeed for shears of 0, 1, 2, and 3 knots/sec. Approximate lines of constant pitch are also drawn. At 160 knots in a no-wind case, for example, the airplane has a pitch attitude of about 16° and climbs at 2132 ft/min (point A in fig. 2). Should the airplane instantaneously encounter a 2 knot/sec shear, the potential climb rate falls to 426 ft/min. To maintain the previous climb rate, the airplane would need to decrease airspeed. This is not directly indicated in figure 2, because the climb-rate curves represent the situation of zero airspeed. Once the stick-shaker speed of about 125 knots is reached, the pilot has no choice but to pitch down to maintain airspeed. The potential climb rate at this speed and shear magnitude is only 74 ft/min (see point B) and would occur at a pitch attitude of about 15°. Had the pilot maintained the initial airspeed of 160 knots (see point C), it would have been necessary to pitch down to about 10°, and the rate of climb would have dropped to 426 ft/min. Had the shear been 3 knots/sec, it would not have been possible to maintain altitude at any constant airspeed.

Recovery Strategies

In this effort, five recovery strategies were developed. The first strategy, pitch attitude, was used as the strategy from which the others evolved. Upon entering the shear, the pitch-attitude strategy drove the airplane pitch attitude toward a target value that remained fixed during the recovery. Initial runs showed that the highest recovery altitude was achieved with a target pitch of 12°, and the target pitch was set at this value for the sensitivity analysis runs.

The second recovery strategy, pitch/vertical-speed hold, evolved from the pitch-attitude strategy. In this strategy, the airplane pitched to an initial target attitude upon entering the shear, as was done in the pitch strategy. Later, as the rate of climb dropped to a specified value, the strategy switched to a control law that held the rate of climb. For the runs to be presented, the specified rate of climb was zero.

In an effort to refine the previous strategy and to develop guidance that would be useful during microburst encounters at very low altitudes, an inertial flight-path-angle recovery strategy was developed. This technique derived a flight-path angle that varied linearly from 1.72° at zero altitude to 0° at an altitude of 100 ft. Above 100 ft, a 0° flight-path angle was targeted. After exiting the shear, a flight-path angle of 60 percent of the potential flight-path angle was targeted to achieve a climb while accelerating the airplane. This flight-path angle was maintained until the pitch attitude was reduced to the initial-climb attitude. A commanded pitch rate was computed to maintain the desired flight-path angle. This scheme had the effect of forcing a climb, regardless of the shear strength, to an altitude of 100 ft to clear immediate obstacles and then holding level flight as long as possible. The altitude of 100 ft is a first approximation of an altitude that would clear obstacles near most airports, and an analysis of departure-path obstacles at air-carrier airports would be needed to refine this altitude.

In an effort to further refine the flight-path-angle strategy, an enhanced flight-path-angle strategy was developed. Evaluation runs showed that, when the airplane entered the shear in certain high-climb-rate situations, the flight-path-angle strategy had poor survivability characteristics. The high climb rates caused the airplane to overshoot the target altitude (100 ft). The flight-path-angle strategy forced the airplane to maintain altitude and decelerate rapidly to the stick-shaker speed, while the pitch strategy produced a descent. The enhanced flight-path-angle strategy also forced a climb to 100 ft, but it could produce intentional descents when above 100 ft. Above 130 ft, the strategy targeted a climb if the potential flight-path angle $\gamma_{i,p}$ were positive (weak or no shear) and targeted a flight-path angle of $K\gamma_{i,p}$ if $\gamma_{i,p}$ were negative. The gain K could be varied from 0, commanding level flight, to 1.0, which commanded a constant-airspeed descent. Initial runs showed that the highest recovery altitude was achieved with a gain of 0.5, and the gain was set at this value for the runs described in this report. Between altitudes of 100 ft and 130 ft, the strategy also targeted a climb if $\gamma_{i,p}$ were positive. If $\gamma_{i,p}$ were negative, a transition from the descent at 130 ft to level flight at 100 ft was produced.

The final strategy developed was the acceleration strategy. This was done in an effort to develop guidance that could feasibly be implemented on airplanes not equipped with inertial reference units. This strategy decelerates the airplane airspeed as a function of the microburst strength. In the evaluation runs conducted with strategies based on pitch

and flight-path angle, the average deceleration of the airplane during successful microburst encounters was about half the horizontal wind rate. This distributed excess kinetic energy across the shear, rather than slowing too rapidly to the stick-shaker speed or failing to use available climb performance.

For this strategy, the previously developed F-factor (eq. (12)) was used to quantify the microburst impact on airplane climb performance as follows:

$$F = \frac{\dot{W}x}{g} - \frac{Wh}{V}$$

The control technique was then governed by the equation

$$\frac{\dot{V}}{g} + \lambda F = 0 \tag{14}$$

where λ is a gain. In a performance decreasing shear, a gain of zero would produce a constant airspeed flight path that would pitch the airplane down and would fail to use available climb performance. A gain of one would produce a constant ground-speed flight path that would pitch the airplane up and rapidly use up the available kinetic energy. Initial runs showed that the highest recovery altitude was achieved with a gain of 0.4, and the gain was set at this value for the sensitivity analysis runs. This control technique could be implemented in numerous ways, such as calculating a target airspeed rate and passing it to an appropriate control law, calculating a target flight-path angle, or calculating a target angle of attack. A control law for calculating a target angle of attack was implemented, and the equations are developed in the appendix.

Batch Simulation of Microburst Encounters

Recovery strategies were developed and evaluated using batch simulations of microburst encounters. A simple point-mass transport-airplane performance model and an analytical wind model based on irrotational, inviscid, point-stagnation flow against a flat plate were programmed. The airplane and microburst models are described in the sections which follow.

Pitch rate was the control used to meet the objectives of each strategy. A limit of 2° per second was applied to the pitch rate, and negative pitch rates were generated as necessary to avoid flight above the stick-shaker angle of attack. The commanded pitch rate was integrated directly to determine airplane pitch attitude.

The airplane was initialized in various initial-climb situations and was flown through the shear. The shear was typically encountered at an altitude of about 75 ft, although different initial conditions were also studied. Only takeoff scenarios were considered in the present effort. Instantaneous shear detection was assumed. The recovery strategy being tested became active immediately upon entering the microburst. Microburst entry is defined subsequently in the discussion of the microburst model.

Batch Simulation Airplane Math Model

The airplane model was based on a Boeing 737-100 flying at a gross weight of 100 000 lb with thrust fixed at 20 000 lbf. The landing gear was retracted and flaps were set at 5°. Thrust, gear position, and flap setting all remained constant during each run.

The stability-axis lift and drag coefficients of the simulated airplane were defined as follows:

$$C_L = C_{L,o} + C_{L_\alpha}\alpha \tag{15}$$

$$C_D = K1 + K2(C_L) + K3(C_L^2) + K4(C_L^3) + K5(C_L^4) \tag{16}$$

where α is in radians and

$$C_{L,o} = 0.2343 \qquad C_{L_\alpha} = 6.1077$$

$$K1 = 0.08009 \qquad K2 = -0.1940 \qquad K3 = 0.3519$$

$$K4 = -0.2238 \qquad K5 = 0.0571$$

The reference wing area for calculating lift and drag is 980 ft^2. Standard sea-level air density was assumed. The equations of motion were developed in reference 5 using the coordinate system shown in figure 1 and are repeated here as follows:

$$\dot{x} = V\cos\ \gamma_a + Wx \tag{17}$$

$$\dot{h} = V\sin\ \gamma_a + Wh \tag{18}$$

$$\dot{W}x = \frac{\partial Wx}{\partial x}\ (\dot{x}) + \frac{\partial Wx}{\partial h}(\dot{h}) + \frac{\partial Wx}{\partial t} \tag{19}$$

$$\dot{W}h = \frac{\partial Wh}{\partial x}\ (\dot{x}) + \frac{\partial Wh}{\partial h}(\dot{h}) + \frac{\partial Wh}{\partial t} \tag{20}$$

$$\dot{V} = \frac{T}{m}\cos\ \alpha - \frac{D}{m} - g\sin\ \gamma_a - \dot{W}x\cos\ \gamma_a - \dot{W}h\sin\ \gamma_a \tag{4}$$

$$\dot{\gamma}_a = \frac{T}{mV}\sin\ \alpha + \frac{L}{mV} - \frac{g}{V}\cos\ \gamma_a + \frac{\dot{W}x}{V}\sin\ \gamma_a - \frac{\dot{W}h}{V}\cos\ \gamma_a \tag{21}$$

Integration was performed with a 0.01-sec step size Δt as follows:

$$x_2 = x_1 + \frac{\Delta t}{2}(3\dot{x}_1 - \dot{x}_0) \tag{22}$$

Microburst Model

The microburst consisted of a simple analytical model based on an axisymmetric flow of an irrotational, inviscid fluid against a flat plate. Two wind components were defined as a function of airplane position and altitude. These were a horizontal component, along the runway axis, and a vertical component. The horizontal wind velocity sheared linearly from a 40-knot head wind to a 40-knot tail wind over a ground distance of 5000 ft. The airplane was considered in the microburst, or in shear, when it was within this 5000-ft region. The vertical downdraft was zero at the surface and varied as a linear function of altitude at the rate of about 5.4 ft/sec per 100 ft. The shear challenged the airplane purely from a performance perspective. No atmospheric turbulence was superimposed on the model.

A solution of the flow in cylindrical coordinates is

$$U = Ar \tag{23}$$

$$Wh = -2Az \tag{24}$$

where r is the radius from the stagnation point, z is the height above the flat plate, and A is the horizontal gradient of the flow. For this effort, the equations were adapted to rectangular coordinates in two dimensions, and the horizontal flow was limited to a finite value beyond an assigned distance from the stagnation point. In rectangular coordinates, the axisymmetric wind components become

$$Wx = Ax \tag{25}$$

$$Wh = -2Ah \tag{26}$$

where x is the distance from the center of the microburst and h is the airplane altitude. For this shear (see fig. 3), the maximum horizontal flow was represented by KW, and the width of the shear was represented by XL. The gradient in the axisymmetric coordinates was then related to KW and XL by

$$A = \frac{KW}{0.5XL} = \frac{2KW}{XL} \tag{27}$$

which yielded

$$Wx = \frac{2KWx}{XL} \tag{28}$$

$$Wh = \frac{-4KWh}{XL} \tag{29}$$

In order to begin the airplane runs at $X = 0$ and to shift the shear along the X-axis, equation (28) was modified; this modification produced the following calculations in the microburst:

$$Wx = \frac{2KW(x - X1)}{XL} - KW \tag{30}$$

$$Wh = \frac{-4KWh}{XL} \tag{31}$$

where $X1$ is the position of the start of the microburst. Prior to reaching $X1$, a constant head wind was provided, and after exiting the shear a constant, tail wind was provided. This representation of a microburst has weaknesses, in that the horizontal wind remains constant to infinity beyond the microburst width, and the vertical wind is the same for all horizontal positions. The model remains useful for this effort, because the shear is encountered very soon after takeoff, the aircraft enters and exits the shear at low altitude, and the recovery is taking place near the center of the shear.

Results and Discussion

The various recovery strategies that were developed had certain characteristics in common. Each strategy determined the pitch attitude necessary to accomplish the objectives of the strategy, then compared that pitch attitude with the actual pitch attitude, and commanded a pitch rate to null the difference. The commanded pitch rate was limited to 2° per second and was integrated directly to define the new pitch attitude. Each strategy also attempted to limit the angle of attack to the value that activated the stick shaker. For the flap setting used in this simulation, the stick-shaker angle of attack was 15°. When the stick-shaker angle of attack was reached, a negative pitch-rate command was generated to reduce the angle of attack. When the angle of attack was reduced below 15°, the airplane attempted to regain the pitch attitude computed by the strategy.

In each case presented, the run began at an altitude of 40 ft, an airspeed of 160 knots, and a nominal 12° pitch attitude. The beginning of the microburst was positioned 500 ft farther along the flight path. A few runs were made with an initial pitch attitude of 16°. In the 12° initial climb pitch case, the encounter with the wind shear began at an altitude of about 75 ft with the airplane climbing 880 ft/min at an airspeed of 163 knots. In each run, the initial climb pitch attitude was maintained until the airplane encountered the shear. Immediately after entering the

shear, the control law automatically switched to the selected recovery strategy. The primary measure of the performance of each recovery strategy is recovery altitude. Recovery altitude is defined as the lowest altitude encountered by the airplane after it has begun to descend in the microburst.

Pitch-Attitude Strategy

The altitude, pitch, and angle-of-attack time histories generated by target pitch attitudes from 10° to 14° are shown in figure 4. In the case of a 10° target pitch attitude, the airplane crashed with excess energy still remaining, the angle of attack was nearly 2° less than the stick-shaker angle of attack and the airspeed was 133 knots, about 10 knots above the 1g stick-shaker speed. The average horizontal shear during the encounter was 3.8 knots/sec. The airplane decelerated, but only at about 1.4 knots/sec. In the case of a 14° target pitch, the airplane initially climbed well, and reached a higher maximum altitude, but reached the stick-shaker angle of attack prior to exiting the shear while descending through 140 ft at over 700 ft/min. The average shear during the climb was 3.3 knots/sec, and the airplane was decelerating at 2.3 knots/sec. The angle of attack was at the stick-shaker limit during the final 9 sec of the flight, and the airspeed increased from a low of 119 knots to the impact speed of 138 knots during this interval. This trajectory with constant angle of attack and varying airspeed is characteristic of the phugoid mode and appears in many of the runs. The best trajectory was obtained with target pitch attitudes of 12° and 13°; only the 12°case is shown. Both attitudes produced recovery altitudes of 10 ft. The 12° recovery occurred without reaching the stick-shaker angle of attack, and the 13° recovery reached the stick-shaker angle of attack for 4 sec. In the 12° run, the average shear during the encounter was 3.6 knots/sec, and the average airplane deceleration was 1.8 knots/sec.

Pitch/Vertical-Speed-Hold Strategy

The time histories generated by initial target pitch attitudes of 10°, 12°, and 14° are shown in figure 5. The initial conditions and shear model for each run were identical to those in the pitch-strategy runs. The plot shows the ability of the airplane to fly through this shear, with only a very slight loss of altitude, to a recovery altitude of 96 ft. This required an initial decrease in pitch attitude to 10°, then a gradual increase in pitch as the airplane slowed in level flight. The maximum pitch achieved was 16.6°, and the stick-shaker angle of attack was reached for 7 sec, beginning 2 sec prior to exiting the shear. The average shear was 3.6 knots/sec and the average airplane deceleration was 1.9 knots/sec. The 12° initial recovery attitude case survived with a recovery altitude of 51 ft, with 11 sec flown at the stick-shaker angle of attack. In the 14° initial attitude case, the stick-shaker angle of attack was reached well before exiting the shear, and the aircraft crashed. This run excited the phugoid mode, and the airspeed increased from a low of 113 knots to the impact speed of 132 knots while flying at the stick-shaker angle of attack.

The effect of unnecessary climbs in the presence of a marginally survivable microburst can be seen. The 12° initial recovery pitch case used more kinetic energy early in the encounter to climb to 148 ft; while the 10° case used less kinetic energy to climb to 108 ft. The extra altitude was quickly lost though, when the stick-shaker angle of attack was reached earlier in the shear.

Flight-Path-Angle Strategy

The time histories generated using the flight-path-angle strategy are shown in figure 6. The initial conditions and shear model were identical to previous runs. The airplane leveled at 100 ft, and the angle of attack reached the stick-shaker limit for 8 sec, beginning just as the shear was being exited. The pitch attitude was initially lowered from 12° to 8° as the shear was entered, and was then increased to 16.4° at the end of the shear, where the stick-shaker angle of attack was reached. The airplane then settled to a recovery altitude of 96 ft before climbing away. The pitch was further increased to 18.5° while maintaining the stick-shaker angle of attack.

A further investigation of the flight-path-angle strategy for recovery from shears encountered very close to the ground was conducted. Trajectories for four takeoff cases are shown in figure 7. In two of the runs, the shear was first encountered while the airplane was still on the ground but in the process of rotating for lift-off. The rotation speed for the math model was set at 148 knots, with actual lift-off in a no-shear takeoff occurring at about 162 knots. The pitch rate was limited to 2°/sec. In run "A", the shear was encountered at an airspeed of 150 knots. The airplane became airborne about 5 sec later, at an airspeed of 149 knots, and climbed to 60 ft prior to reaching the stick-shaker angle of attack. The angle of attack remained at 15° until impact.

In run "B", the encounter airspeed was 156 knots. The airplane became airborne 2 sec later and was able to climb to a height of 70 ft prior to reaching the stick-shaker angle of attack. The stick-shaker angle of attack was reached just prior to the end of the shear, and the airplane settled to a height of 19 ft before resuming a climb. The airplane became

airborne at a pitch of 10°, and generally continued to increase in pitch to a maximum of 16.4° prior to reaching stick shaker. The average shear during the climb was 3.8 knots/sec, and the average airspeed deceleration was 1.9 knots/sec.

In run "C", the shear was initially encountered at an altitude of only 5 ft, at an airspeed of 163 knots, and at a pitch attitude of 12°. The pitch was slightly reduced to 8.5° to limit the rate of climb, and was then increased smoothly to 16.5° as the airplane slowed and climbed to 80 ft. The stick-shaker angle of attack was reached for about 7 sec, beginning just as the shear was exited. The average shear during the climb was 3.6 knots/sec and the average airspeed deceleration was 1.9 knots/sec.

In run "D", the shear was encountered at an altitude of 20 ft, at an airspeed of 165 knots, and at a pitch attitude of 14°. The pitch was initially reduced to 7.5° to reduce the rate of climb, and was then gradually increased to a maximum of 18.8°. The airplane flew at the stick-shaker angle of attack for about 7 sec. The average shear and airspeed rates were 3.8 and 2.0 knots per sec, respectively. The initial pitch reduction at low altitude may seem counterproductive, but had it not occurred, the stick-shaker angle of attack would have been reached with more shear remaining, and greater altitude loss would have resulted. The results of this and other efforts (ref. 5) can be interpreted to indicate that if a recovery requires the use of stick-shaker angle of attack, that angle of attack should not be reached until the end of the shear for optimum performance. Since the location of the end of the shear is not known in an actual encounter, flight at the stick-shaker angle of attack must be postponed as long as possible.

Enhanced Flight-Path-Angle Strategy

The enhanced flight-path-angle strategy produced the same results as the simple flight-path-angle strategy when tested in the same shear with the same initial conditions. Both produced a recovery altitude of 96 ft. The results are the same because the airplane never reached the higher altitudes, where the strategies differ. As is discussed in the section "Sensitivity of Strategies to Shear Encounter Variations," the enhanced flight-path-angle strategy did perform much better than the original flight-path-angle strategy in other scenarios.

Acceleration Strategy

The time histories produced by the acceleration strategy for various gains are shown in figure 8. Gains of 0.0, 0.4, 0.5, and 1.0 are plotted. The flight with the gain equal to 0.0 produced an immediate pitch-down from 12° to 4° after shear entry. The airspeed decreased from 163 knots to 158 knots during the reduction in pitch, and then remained at 158 knots to impact. The speed loss was partially the result of the pitch-rate limit of 2°/sec. At the other extreme, a gain of 1.0 produced an initial pitch-up from 12° to about 27°, where the stick-shaker angle of attack was reached. The airplane then began to pitch down, in an attempt to limit the angle of attack, and continued to pitch down until impact. The pitch-rate limit prevented the control law from maintaining the stick-shaker angle of attack, and an angle of attack of 21.5° was reached during the descent. A minimum airspeed of 97 knots was reached. These plots are shown only to illustrate the extremes in airplane energy distribution across the shear. Gains of 0.4 and 0.5 produced successful flight paths. Gains at or below 0.3 and at or above 0.6 resulted in crashes. With a gain of 0.4, the recovery altitude was 46 ft. Upon entering the shear, the airplane initially pitched down from 12° to 8.8°, before smoothly pitching up to 14°, where the stick-shaker angle of attack was reached. The stick-shaker angle of attack was reached while exiting the shear, and the airplane continued pitching up, while maintaining the stick-shaker angle of attack, to 20°. The minimum airspeed reached was 127 knots. The average deceleration during the shear was 1.7 knots/sec, and the average horizontal shear was 3.9 knots/sec. The ratio of airplane deceleration to horizontal shear was slightly higher than the gain, because the control law also included the effects of vertical winds.

When the gain was increased to 0.5, the recovery altitude decreased to 41 ft. The airplane initially pitched down from 12° to 10.8° before smoothly pitching up to 16.5°, where the stick-shaker angle of attack was reached (about 3 sec prior to exiting the shear). The stick-shaker angle of attack was maintained for 14 sec. The recovery altitude was reached while at the stick-shaker angle of attack. The minimum airspeed was 117 knots. The average deceleration was 2.2 knots/sec, and the average shear was 3.8 knots/sec.

Sensitivity of Strategies to Shear Encounter Variations

In an effort to determine the robustness of the various strategies to variations in the microburst encounters, runs were made with an initial-climb pitch of 16° and with 5 percent weaker and stronger shears. All previous runs were made with an initial-climb attitude of 12°. A 16° pitch attitude is more typical of a normal climb where wind shear is not expected. All previous runs were made with a change in horizontal wind of 80 knots. Additional runs were made with total shears of 76 knots and 84 knots.

The length of the shear remained constant, and the vertical winds were scaled with the horizontal wind magnitude.

The effect on recovery altitude of varying the initial-climb pitch and shear entry altitude is shown in figure 9. Increasing the initial-climb pitch increased the altitude at which the shear was entered, from about 75 ft to 122 ft (since the airplane enters the shear after flying 500 ft from the initial point), and increased the rate of climb at shear entry, from 876 ft/min to about 1800 ft/min.

The higher initial-pitch attitude slightly increased the recovery altitude of the pitch strategy, from 10 ft to 13 ft (fig. 10), but significantly lowered the recovery altitude of all other strategies. Although the pitch strategy recovered at a slightly higher altitude with an initial pitch of 16°, the recovery required flying at the stick-shaker angle of attack for 6 sec. In the 12° initial-pitch case, the stick-shaker angle of attack was never reached during the recovery.

The two strategies that simply attempt to hold altitude, the pitch/vertical-speed strategy and the simple flight-path-angle strategy, crashed when the steeper initial climb was used. The time histories for these two strategies are nearly identical, and the time histories produced by the simple flight-path-angle strategy are shown in figure 11. With the lower initial-climb pitch, these two laws had the best performance with recovery altitudes of 96 ft. The difference is that in the 12° initial-pitch runs, these strategies quickly arrested the climb at an altitude of 100 ft to 110 ft and then maintained level flight. In the 16° runs, the climb was not arrested until the airplane had climbed to about 190 ft. The airplane lost about 5 knots more speed while arresting the steep climb than was lost arresting the shallow climb. The airplane attempted to maintain altitude in the stronger downdraft at the higher altitude, and the excess potential energy was not used to maintain kinetic energy. The stick-shaker angle of attack was reached about 5 sec before exiting the shear, and a phugoid cycle began. Even though the airplane exited the shear at an altitude of about 140 ft and airspeed was increasing, impact could not be prevented.

The performance of the acceleration strategy (fig. 12) was also degraded by the higher initial-climb pitch, but to a lesser degree. The minimum recovery altitude was reduced from 46 ft to 21 ft. This strategy also arrested the climb at a higher altitude, up from 110 ft to 192 ft, but then allowed a descent to convert this excess potential energy to airspeed. By the time the stick-shaker angle of attack was reached, the airplane had descended to 130 ft and was 3 sec from exiting the shear.

The enhanced performance of the flight-path-angle strategy is shown in figure 13 and was degraded less severely by the steeper climb. The minimum recovery altitude was reduced from 96 ft to 82 ft. This strategy also arrested the climb at a higher altitude (191 ft) in the steep climb case than in the shallow initial-climb case (100 ft), and initiated an immediate descent to 100 ft. The airplane had rotated to stop the descent at 100 ft, and was 1 sec from exiting the shear, when the stick-shaker angle of attack was reached. This angle of attack was maintained as the airplane settled to 82 ft and began to climb away.

The effect on recovery altitude of varying the shear strength is shown in figure 14. The two strategies, pitch and acceleration, that do not close a loop on altitude or flight-path angle show a large sensitivity to both a 5-percent decrease and a 5-percent increase in shear strength. The recovery altitude of the pitch law (fig. 15) was increased 24 ft (240 percent) with the weaker shear. The airplane did not recover in the stronger shear. The recovery altitude of the acceleration strategy (fig. 16) increased 29 ft (63 percent) with the weaker shear and decreased 31 ft (67 percent) with the stronger shear.

The three strategies that control rate of climb or flight-path angle showed very little sensitivity to reduced microburst strength, but showed sensitivity to the increased microburst strength that was similar to that for the pitch and acceleration strategies. The histories produced by the enhanced flight-path-angle strategy are shown in figure 17. With the weaker shear, the recovery altitudes were only increased by 4 ft to 13 ft (4 percent to 14 percent), because the strategy could not predict that the airplane would exit the shear with more airspeed margin than necessary and did not use all the available energy to climb. The recovery altitudes were reduced by 44 ft to 54 ft (46 percent to 56 percent) by the stronger shear. Compared with the pitch or acceleration strategies, the flight-path-angle strategies produced a larger reduction in recovery altitude with the stronger shear. However, recovery still occurred at a much higher altitude, and the percent change in recovery altitude was smaller. The average change in recovery altitude for all strategies was 60 percent.

In general, the effect of the shear strength on recovery altitude change is related to the occurrence of stick-shaker angle of attack just as the airplane is exiting the shear. In the critical midstrength shear, the airplane had enough energy to delay reaching the stick-shaker angle of attack until just prior to exiting the shear. The airplane then developed a sink rate, but was able to accelerate and recover after exiting the shear. By slightly reducing the strength of the shear, the limiting angle of attack was not reached

until the airplane exited the shear, time spent at stick-shaker angle of attack was reduced, and the sink rate did not develop. By slightly increasing the shear strength, the limiting angle of attack occurred sooner, and the phugoid mode became well developed before exiting the shear.

Concluding Remarks

Since the microburst exists over a given distance, and since the airplane total-energy rate is negative while traveling that distance, the best recovery procedure (from a performance perspective) minimizes the time spent in the shear and keeps the airplane flying above the stick-shaker airspeed for the greatest possible ground distance. Any unnecessary climb reduces the airplane speed excessively, increases the time spent in the shear, places the airplane in a stronger downflow, and leads to earlier stick-shaker activation. With no knowledge of how long the shear will last, the activation of stick shaker must be delayed as long as possible, because at that point the airplane phugoid mode is excited and a descent can no longer be prevented.

The characteristics of a recovery procedure that best utilizes available airplane energy in a takeoff microburst encounter include an initial reduction in pitch attitude early in the encounter to reduce the climb rate, an increase in pitch-up to stick-shaker angle of attack late in the encounter, the smallest angle of climb necessary for obstacle clearance, and, if at a higher altitude than necessary, an intentional descent to reduce the airspeed deceleration. The rate of descent should be small and should be varied with airplane altitude to prevent undershooting a given minimum altitude.

In this study, the strategies that produced the highest recovery altitudes were the ones that were based on altitude rate or flight-path-angle control. The pitch strategy and the acceleration strategy produced the lowest recovery altitudes and the greatest sensitivities to changes in shear strength or airplane initial conditions. The altitude-rate and flight-path-angle strategies produced the highest recovery altitudes and the lowest sensitivities to changes in shear strength or airplane initial conditions. Minimum altitudes reached during recoveries were, in general, very sensitive to small changes in microburst strength; 5-percent changes in shear strength produced an average 60-percent change in recovery altitude. The enhanced flight-path-angle strategy had the best overall performance.

The results indicate that recovery procedures based on flight-path angle are the most promising, and that additional research is needed in this area. In particular, the research needs to address (a) using in situ and look-ahead wind-shear data to predict the climb angle that is possible in a given encounter, (b) the effects of turbulence and more complex shear structures on the recovery strategies, (c) piloting factors such as guidance display options and the ability to follow the guidance, (d) airline and Federal Aviation Administration procedural policies and regulations, and (e) the actual obstacle clearance requirements at airports. Extension of the work to the approach-to-landing case is also necessary.

NASA Langley Research Center
Hampton, Virginia 23665-5225
July 1, 1988

Appendix

Acceleration Strategy Control Law

One guidance strategy tested was based on decelerating the airplane as a function of the microburst strength. The microburst strength is defined by the "F-factor," which describes the change in airplane potential flight-path angle caused by the horizontal wind rate and the vertical wind magnitude. The F-factor is defined as

$$F = \frac{\dot{W}x}{g} - \frac{Wh}{V} \tag{A1}$$

The governing equation for the control technique then becomes

$$\frac{\dot{V}}{g} + \lambda F = 0 \tag{A2}$$

One method of controlling speed rate is to control the drag term in the potential climb-angle equation by controlling angle of attack. The derivation begins with

$$\gamma_{a,p} = \frac{(T-D)}{W} - \frac{\dot{W}x}{g} \tag{A3a}$$

or

$$\frac{T-D}{W} - \gamma_{a,p} - \frac{\dot{W}x}{g} = 0 \tag{A3b}$$

The difference between the potential climb angle and the actual climb angle is

$$\gamma_{a,p} - \gamma_a = \frac{\dot{V}}{g} \tag{A4}$$

Solving for $\gamma_{a,p}$ and substituting into equation (A3b) gives

$$\frac{T-D}{W} - \left(\gamma_a + \frac{\dot{V}}{g}\right) - \frac{\dot{W}x}{g} = 0 \tag{A5}$$

and setting $\frac{\dot{V}}{g} = -\lambda F$ gives

$$\frac{T-D}{W} - \gamma_a + \lambda F - \frac{\dot{W}x}{g} = 0 \tag{A6}$$

Substituting the definition of F yields

$$\frac{T-D}{W} - \gamma_a - (1-\lambda)\frac{\dot{W}x}{g} - \frac{\lambda Wh}{V} = 0 \tag{A7}$$

If

$$(1-\lambda)\frac{\dot{W}x}{g} + \frac{\lambda Wh}{V} = G \tag{A8}$$

then equation (A7) simplifies to

$$\frac{T-D}{W} - \gamma_a - G = 0 \tag{A9}$$

A target drag value can now be defined as

$$D = T - W(\gamma_a + G) \tag{A10}$$

where thrust and weight are fixed, γ_a and G are independent variables, and G is a function of the gain λ and the wind-shear strength. The drag is assumed to be in the form

$$D = Sq\left(C_{D,o} + \frac{\partial C_D}{\partial \alpha}\alpha + \frac{\partial C_D}{\partial \alpha^2}\alpha^2\right) \tag{A11}$$

which, when combined with the equation (A10), gives

$$C_{D,o} + \frac{\partial C_D}{\partial \alpha} + \frac{\partial C_D}{\partial \alpha^2}\alpha^2 = \frac{T - W(\gamma_a + G)}{Sq} \tag{A12}$$

Solving for angle of attack with the quadratic formula yields

$$\alpha = \frac{-\frac{\partial C_D}{\partial \alpha} \pm \sqrt{\left(\frac{\partial C_D}{\partial \alpha}\right)^2 - 4\frac{\partial C_D}{\partial \alpha^2}\left(C_{D,o} - \frac{T - W(\gamma_a+G)}{Sq}\right)}}{2\frac{\partial C_D}{\partial \alpha^2}} \tag{A13}$$

This solution cannot be used directly, because the square root may produce complex results and two values of angle of attack are produced. Fortunately, the term under the square-root sign can be limited to nonnegative values, and only the larger of the two angle-of-attack values is reasonable. This process produces the solution

$$\text{TEMP} = \left(\frac{\partial C_D}{\partial \alpha}\right)^2 - 4\frac{\partial C_D}{\partial \alpha^2}\left(C_{D,o} - \frac{T - W(\gamma_a + G)}{Sq}\right) \tag{A14}$$

If TEMP in equation (A14) is less than or equal to zero, then TEMP is set equal to zero. The nonnegative limit on the term under the square-root sign was tested in shear to determine when it was active. The limiting only took place during initial pitch-down maneuvers upon shear entry, while the airplane was pitching down its limit pitch rate. The nonnegative term limit was therefore not affecting the results obtained with this strategy.

For this simulation, the partial derivatives of the drag coefficient were estimated for the angle-of-attack range of interest (about 6° to 16°) to be

$$C_{D,o} = 0.07177$$

$$\frac{\partial C_D}{\partial \alpha} = -0.378$$

$$\frac{\partial C_D}{\partial \alpha^2} = 2.951$$

where angle of attack was expressed in radians. The computed angle-of-attack goal was compared with the actual angle of attack to determine pitch error, which was used to generate a pitch rate on the airplane.

References

1. McCarthy, John; Blick, Edward F.; and Bensch, Randall R.: *Jet Transport Performance in Thunderstorm Wind Shear Conditions.* NASA CR-3207, 1979.
2. Fujita, T. Theodore: *The Downburst—Microburst and Macroburst.* SMRP-RP-210, Univ. of Chicago, 1985. (Available from NTIS as PB85 148 880.)
3. Psiaki, Mark L.; and Stengel, Robert F.: Analysis of Aircraft Control Strategies for Microburst Encounter. AIAA-84-0238, Jan. 1984.
4. Psiaki, Mark L.; and Stengel, Robert F.: Optimal Flight Paths Through Microburst Wind Profiles. *J. Aircr.*, vol. 23, no. 8, Aug. 1986, pp. 629–635.
5. Miele, A.; Wang, T.; and Melvin, W. W.: Optimal Take-Off Trajectories in the Presence of Windshear. *J. Optim. Theory & Appl.*, vol. 49, no. 1, Apr. 1986, pp. 1–45.
6. Miele, A.; Wang, T.; and Melvin, W. W.: *Maximum Survival Capability of an Aircraft in a Severe Windshear.* Aero-Astronaut. Rep. No. 213, Rice Univ., 1986.
7. Miele, A.; Wang, T.; and Melvin, W. W.: *Gamma Guidance Schemes and Piloting Implications for Flight in a Windshear.* Aero-Astronaut. Rep. No. 212, Rice Univ. 1986.
8. Ostroff, Aaron J.; Hueschen, Richard M.; Hellbaum, R. F.; Belcastro, Christine M.; and Creedon, J. F.: *Evaluation of a Total Energy-Rate Sensor on a Transport Airplane.* NASA TP-2212, 1983.

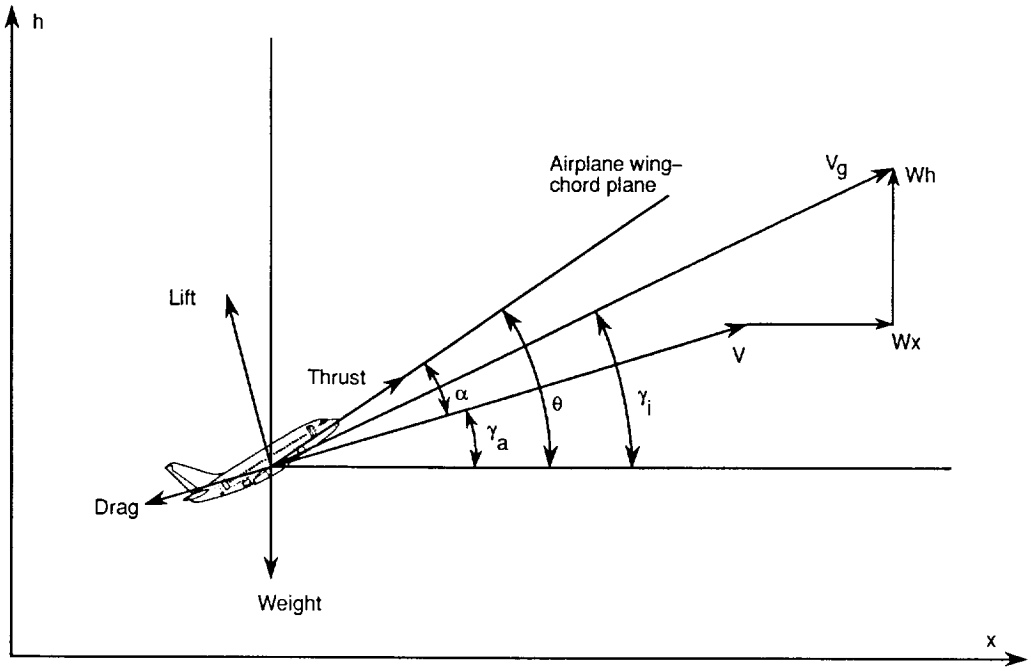

Figure 1. Flight path and wind coordinate system.

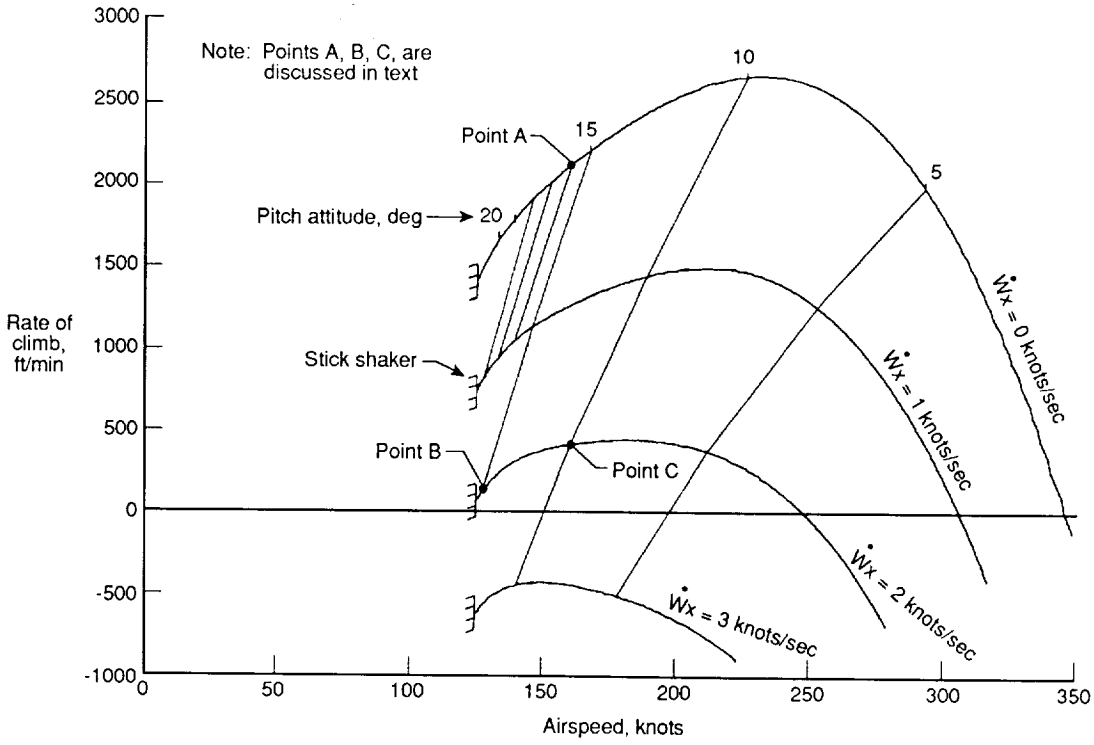

Figure 2. Constant-speed climb performance in wind shear.

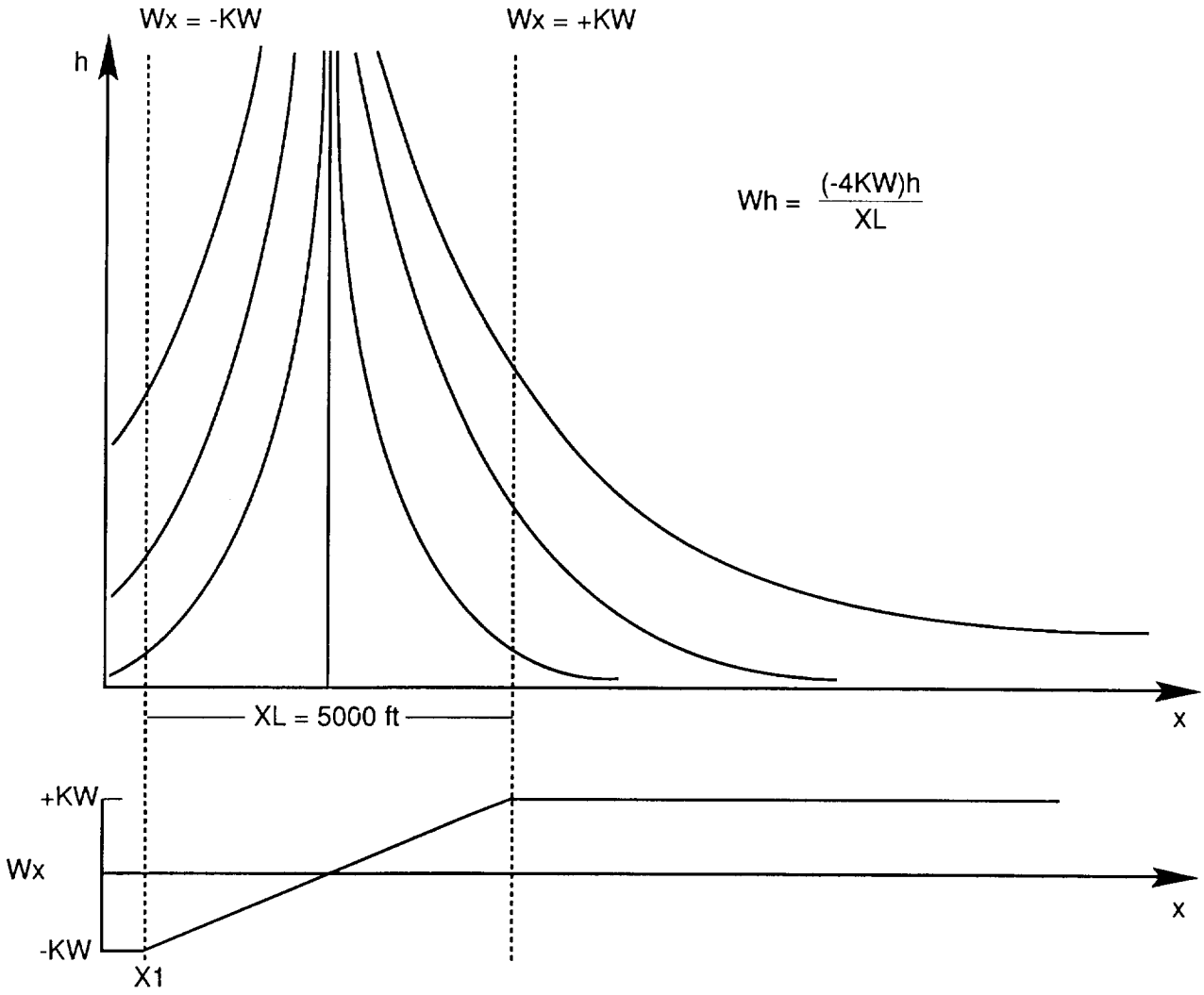

Figure 3. Wind-shear model.

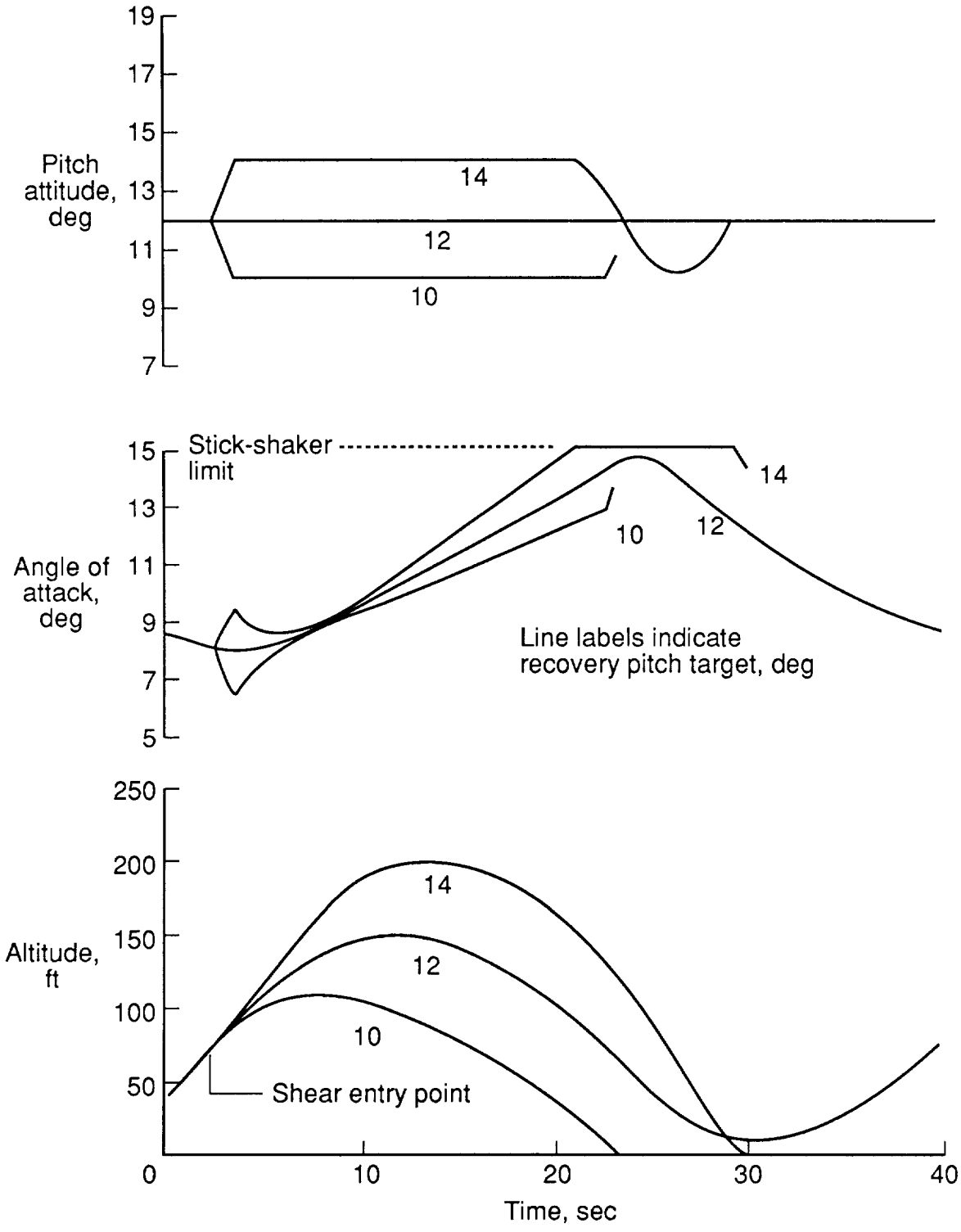

Figure 4. Pitch-attitude recovery strategy with three recovery attitude targets.

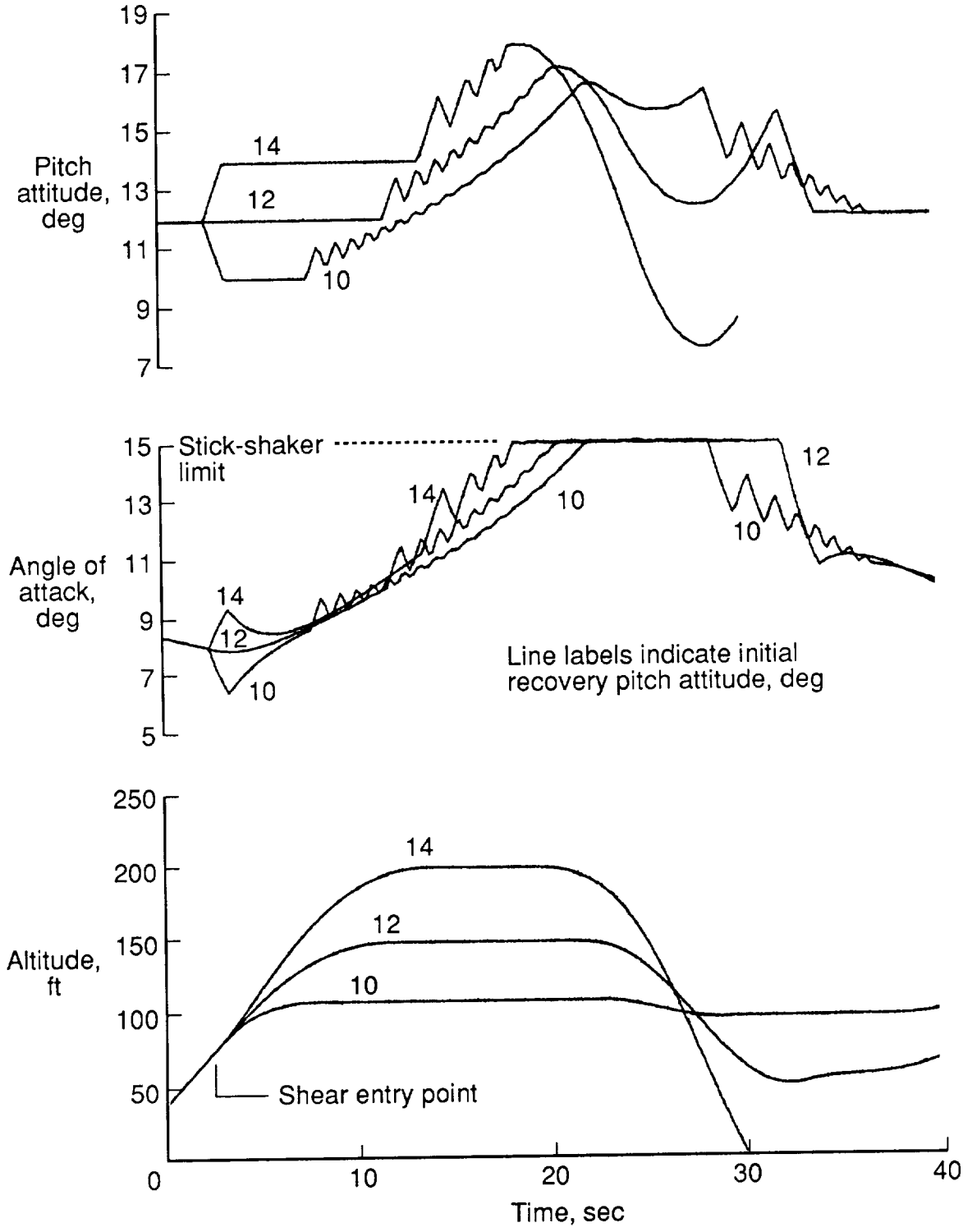

Figure 5. Pitch/vertical-speed-hold strategy with three initial recovery pitch attitudes.

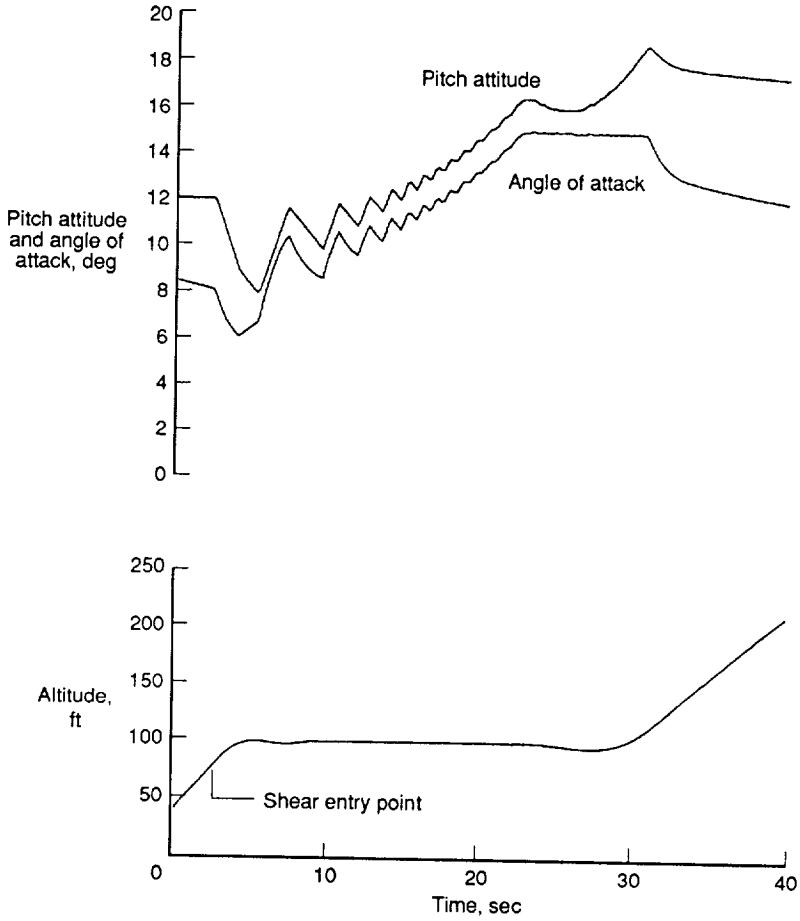

Figure 6. Flight-path-angle strategy.

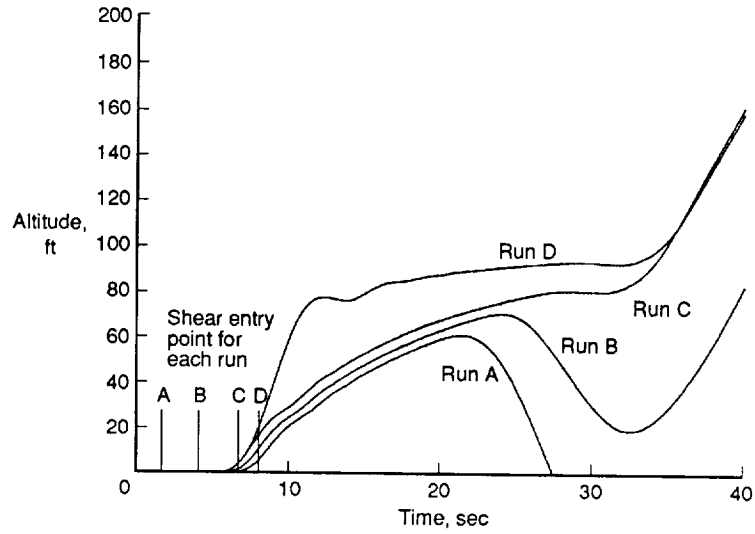

Figure 7. Flight-path-angle strategy in four very low altitude wind-shear encounters.

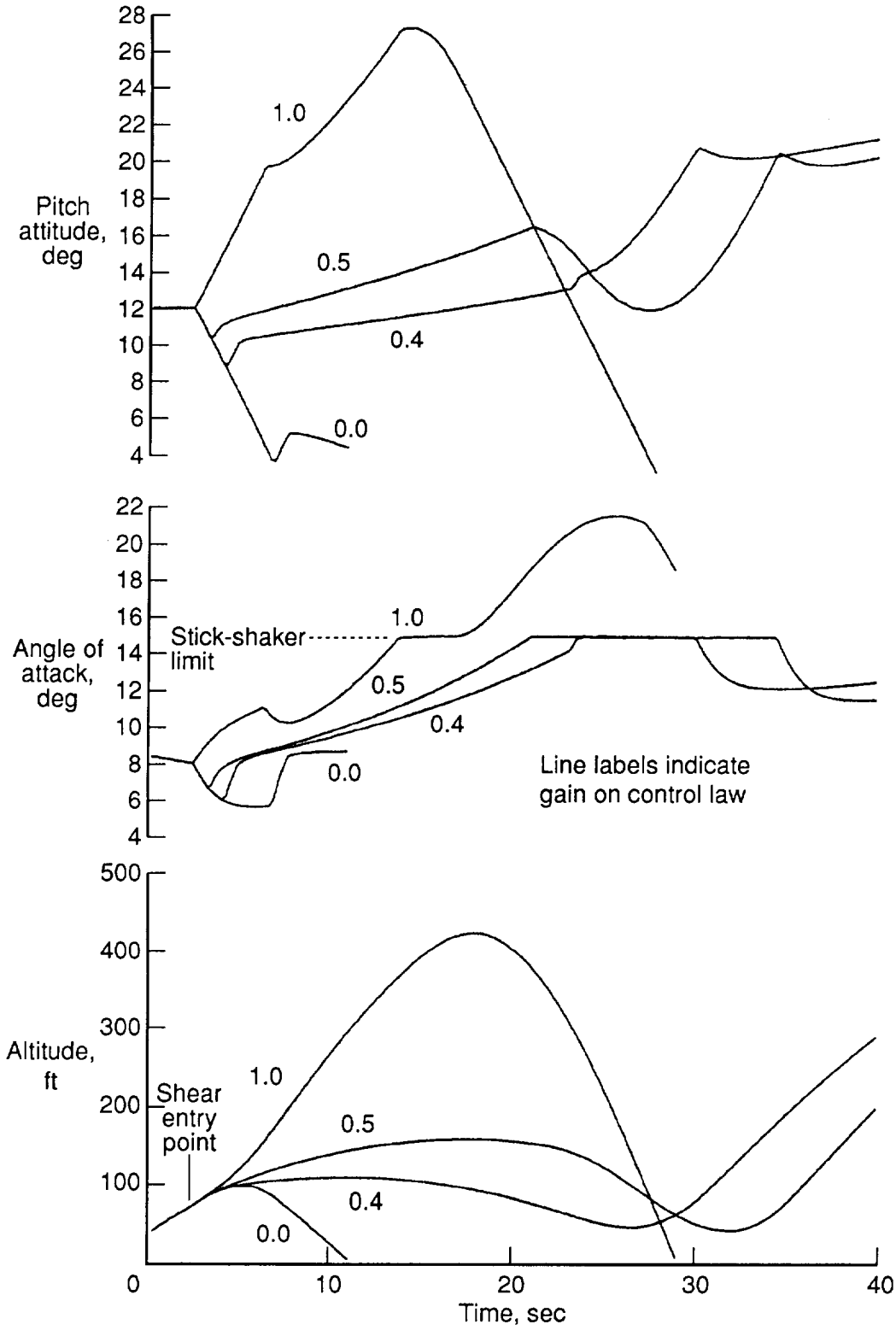

Figure 8. Acceleration strategy with various gains.

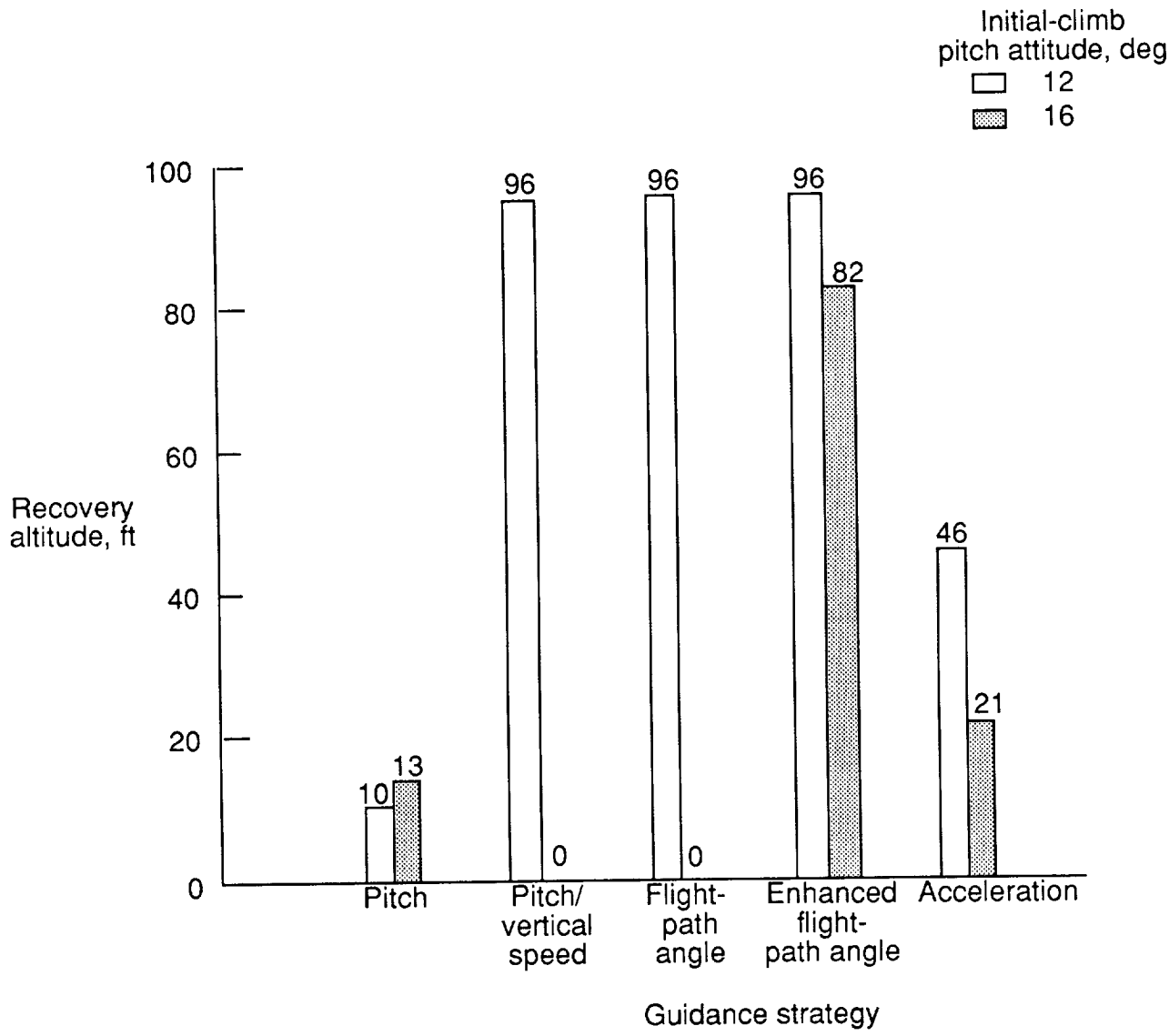

Figure 9. Effect of initial aircraft climb pitch on recovery altitude.

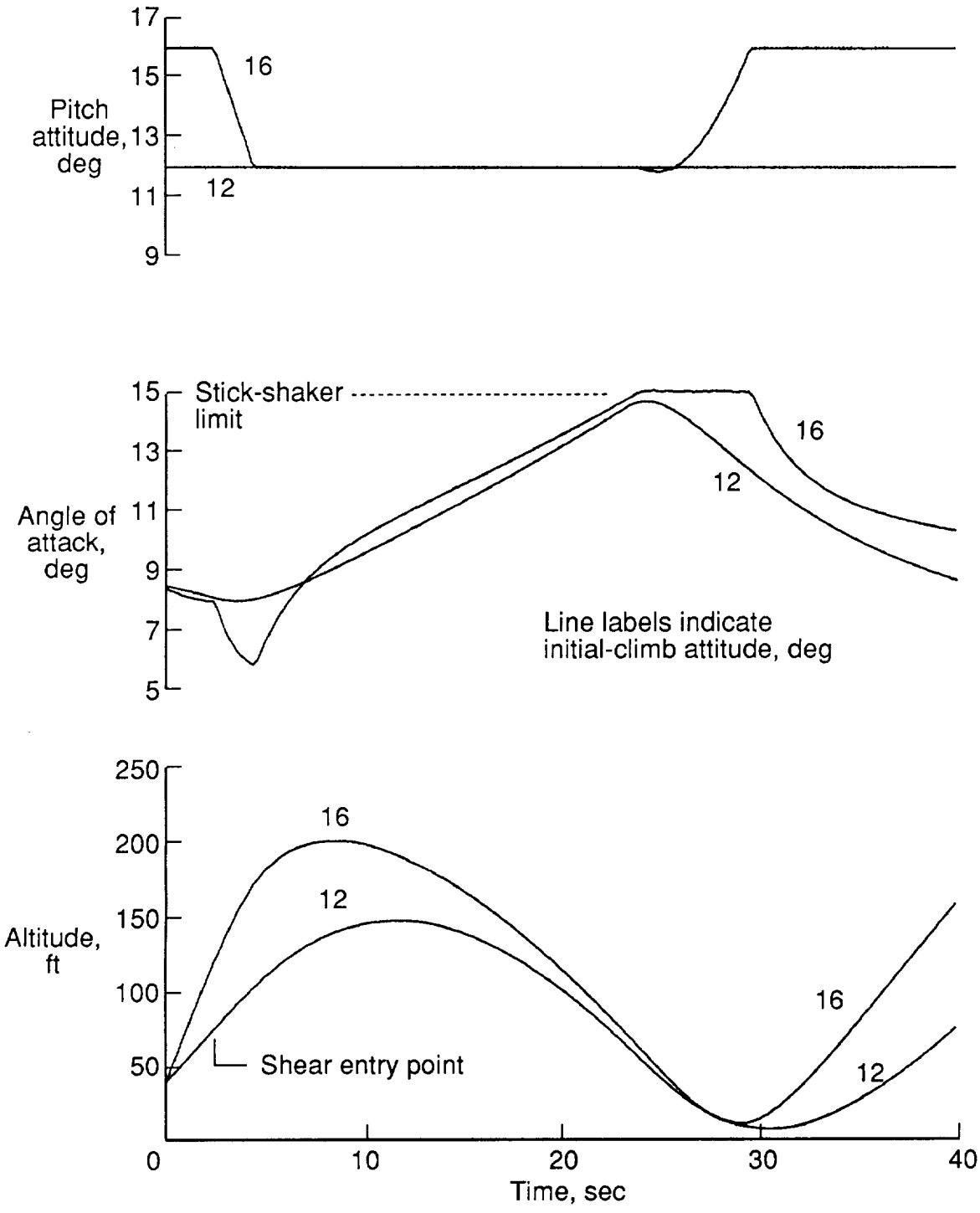

Figure 10. Pitch-attitude strategy with two initial-climb pitch attitudes.

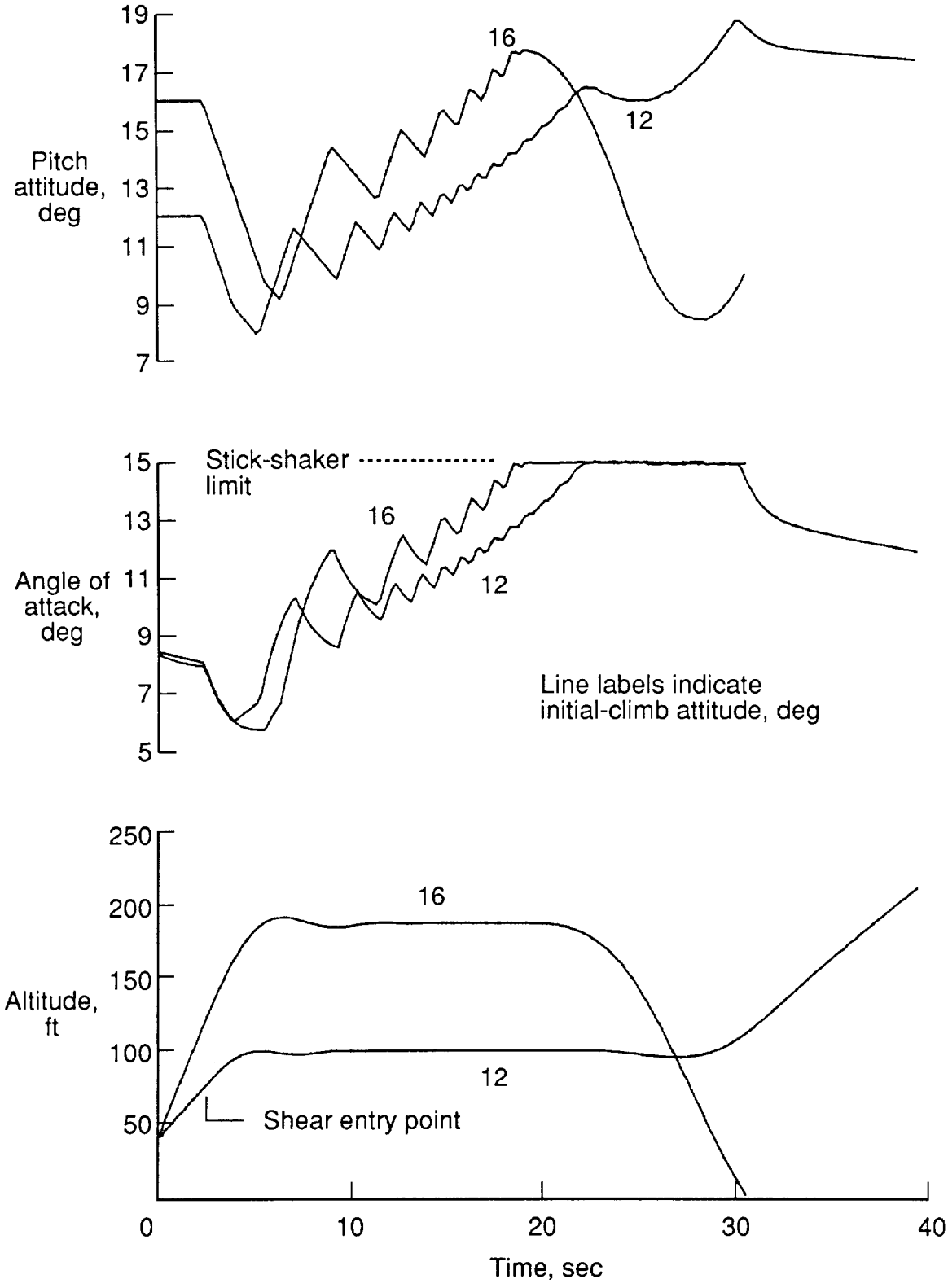

Figure 11. Flight-path-angle strategy with two initial-climb pitch attitudes.

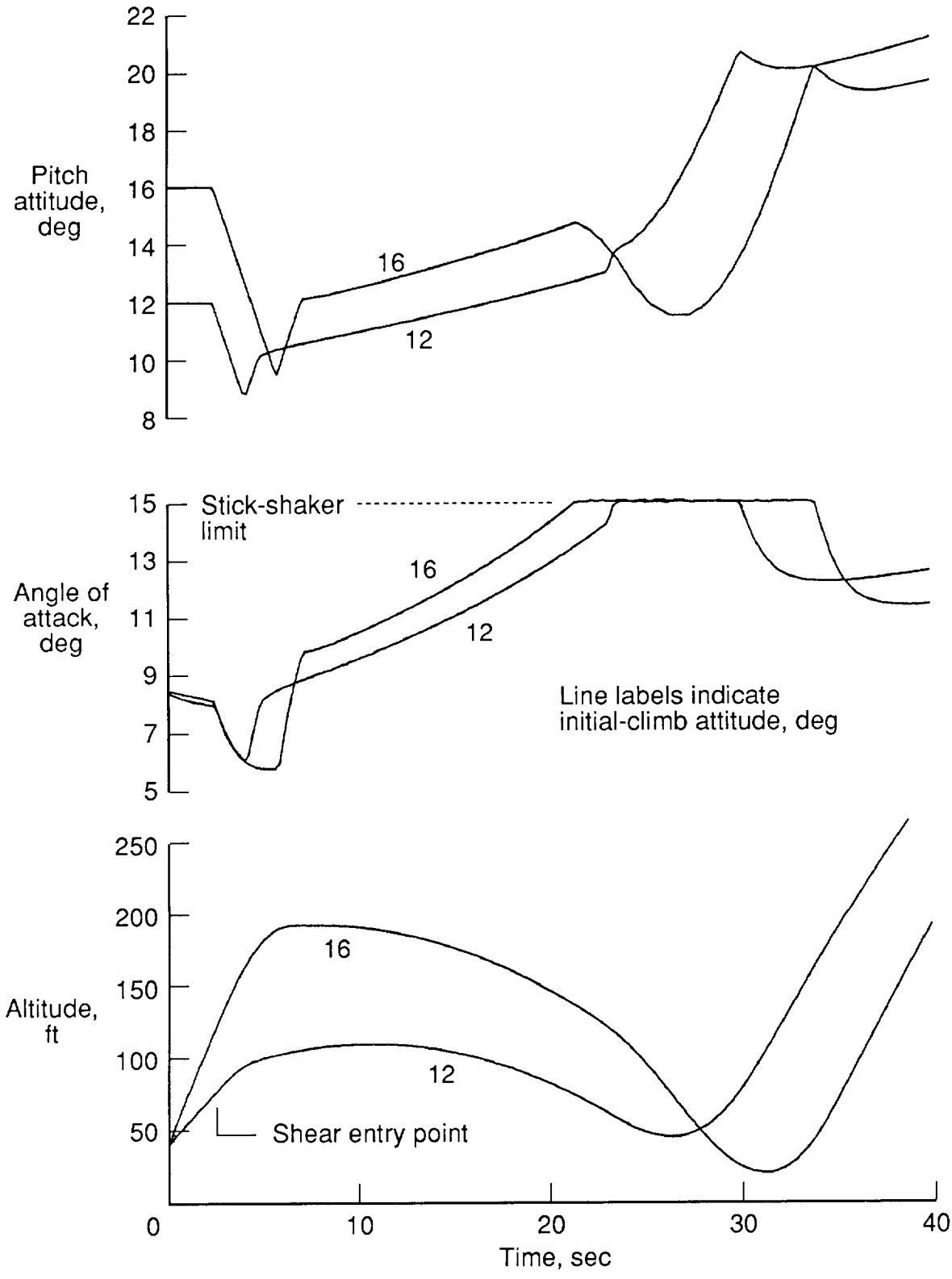

Figure 12. Acceleration strategy with two initial-climb pitch attitudes.

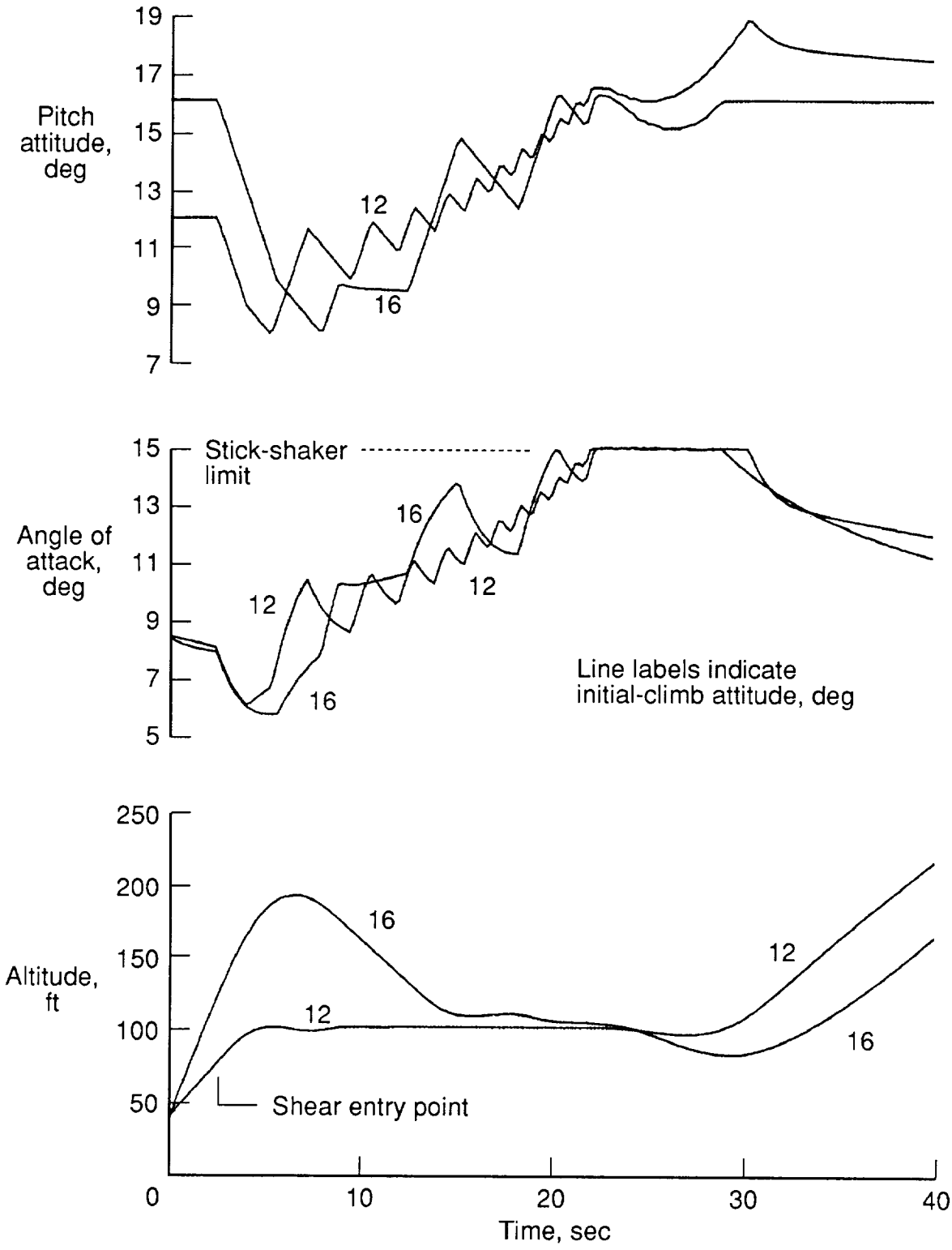

Figure 13. Enhanced flight-path-angle strategy with two initial-climb pitch attitudes.

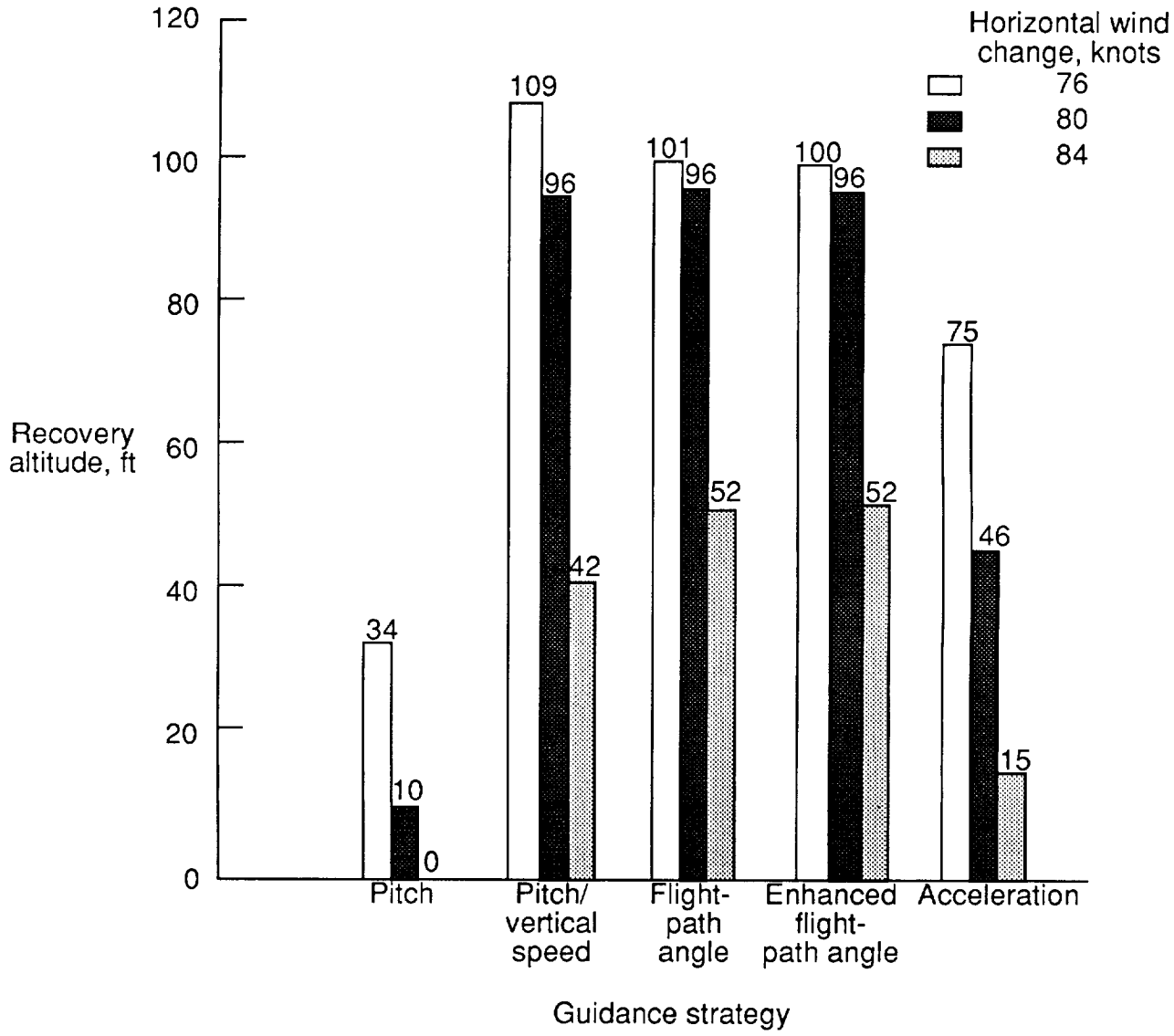

Figure 14. Effect of horizontal wind-change magnitude variation on recovery altitude.

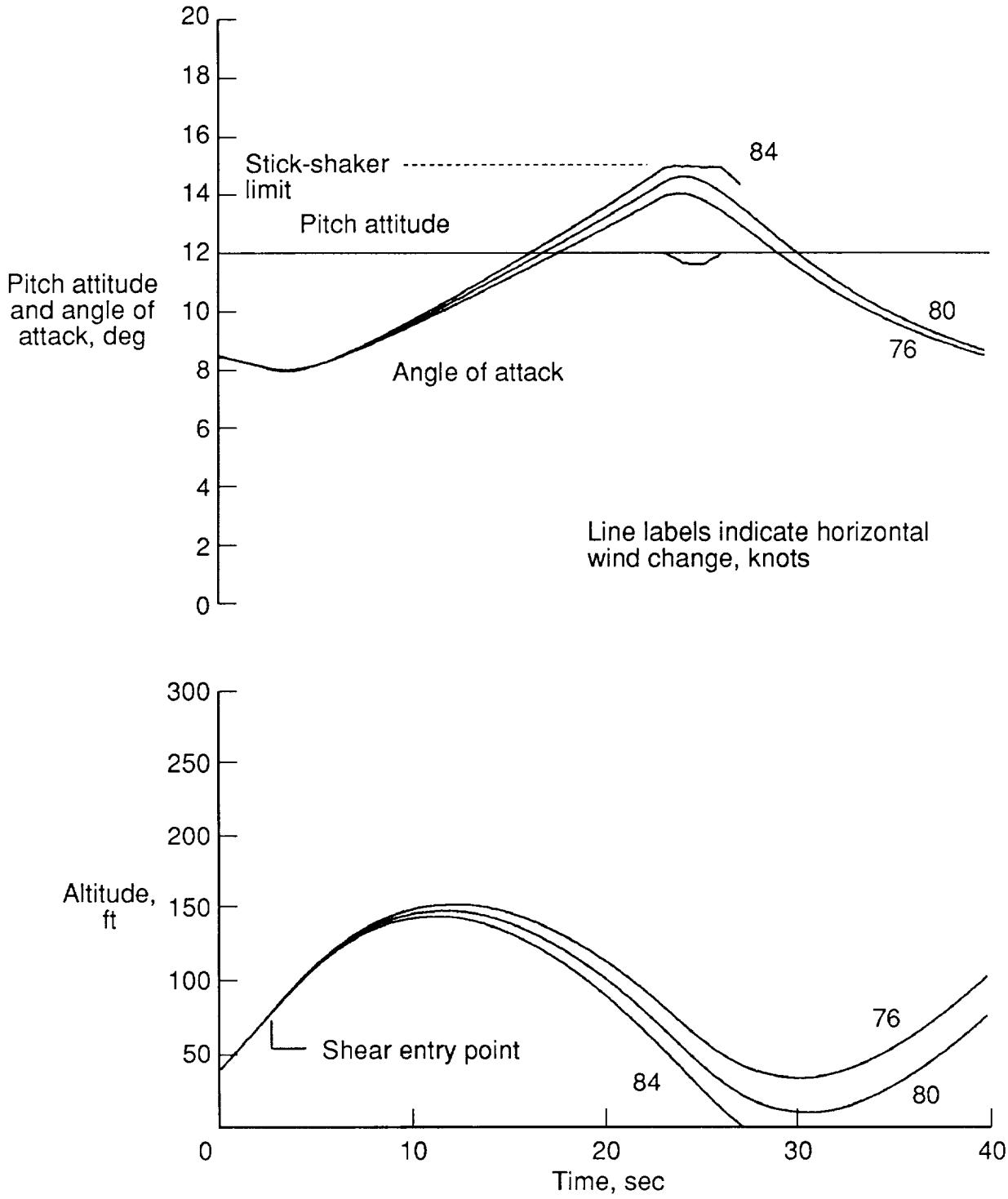

Figure 15. Pitch-attitude strategy with three wind-shear magnitudes.

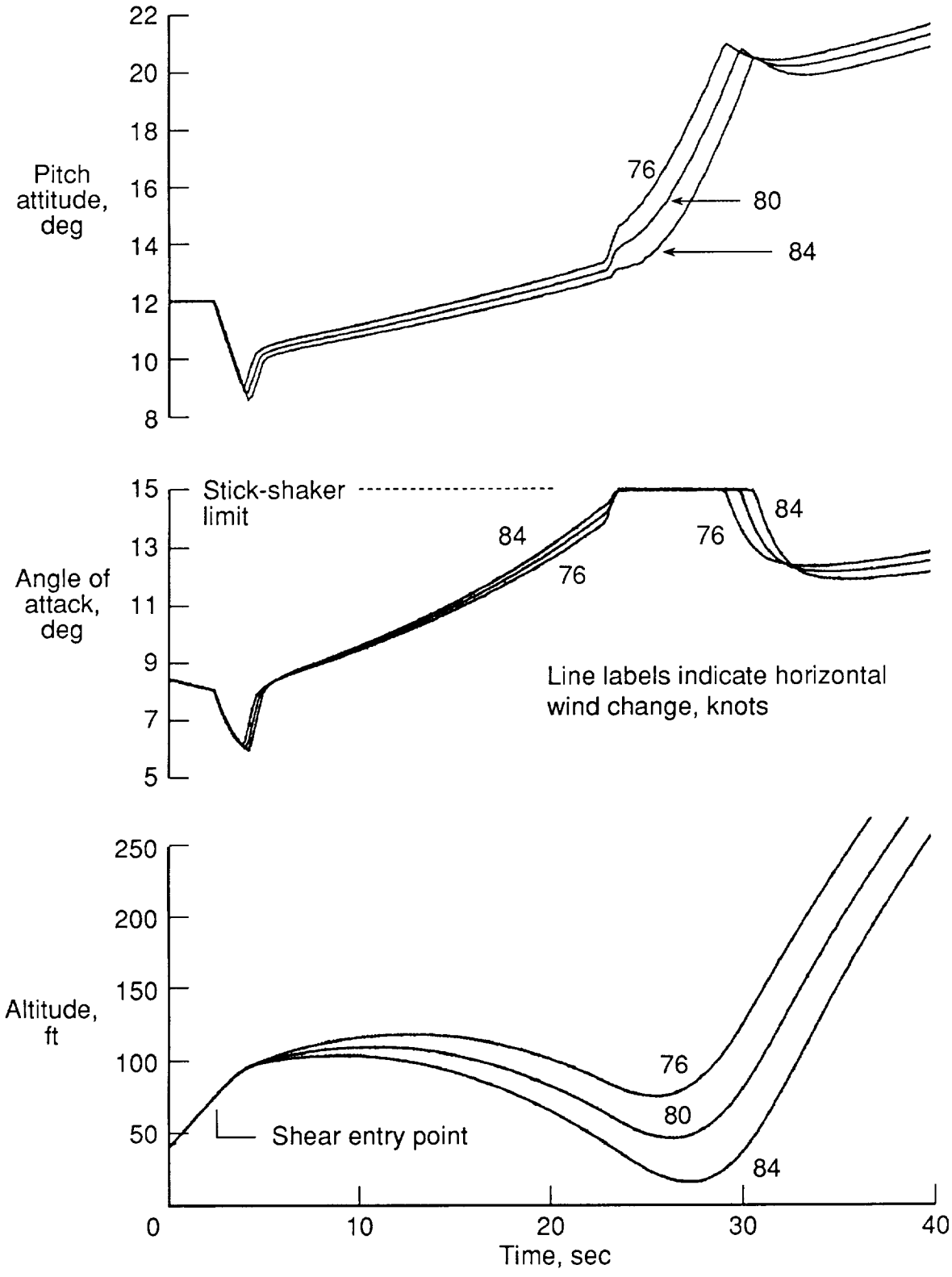

Figure 16. Acceleration strategy with three wind-shear magnitudes.

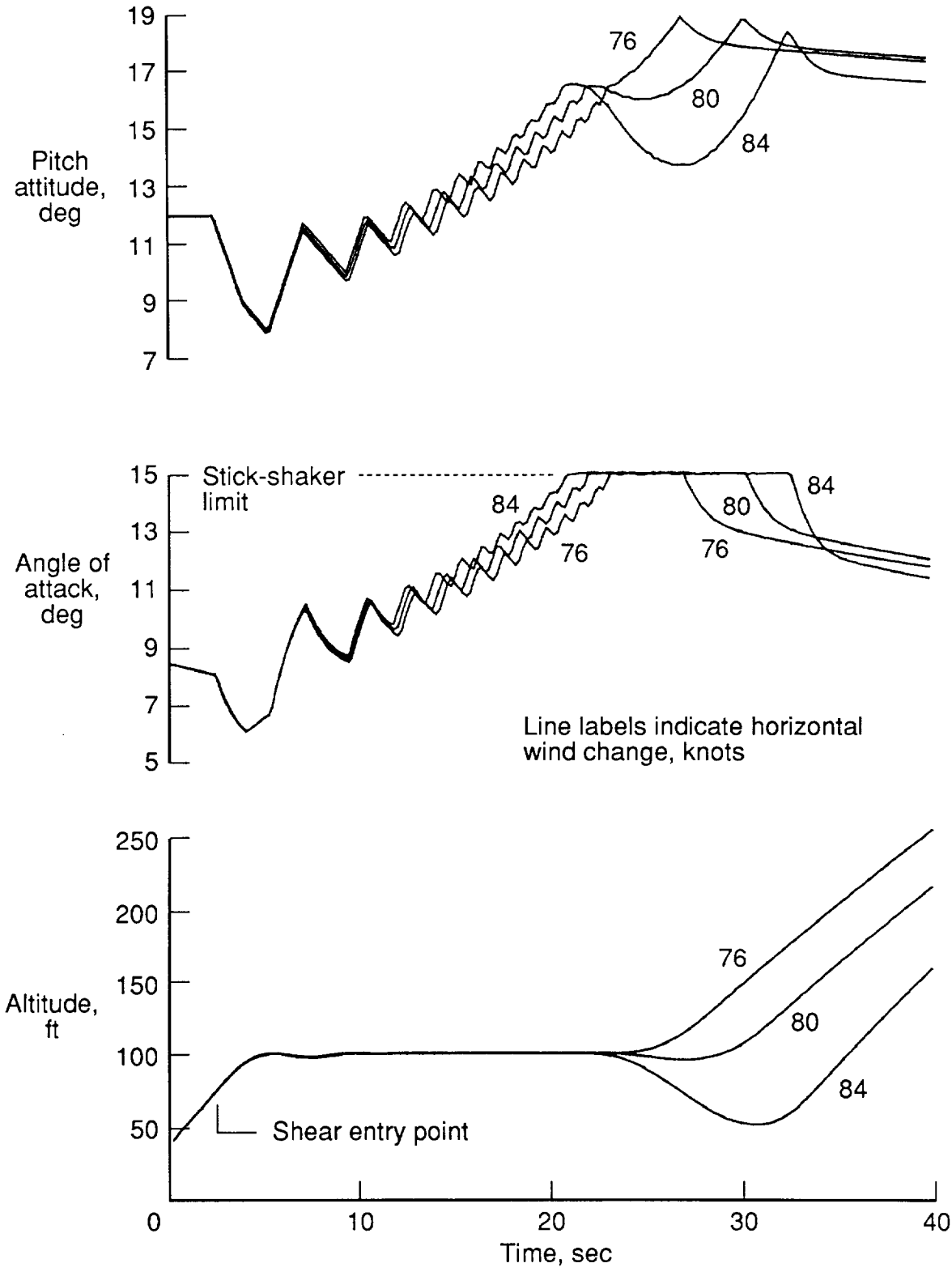

Figure 17. Enhanced flight-path-angle strategy with three wind-shear magnitudes.

NASA
National Aeronautics and Space Administration

Report Documentation Page

1. Report No.	2. Government Accession No.	3. Recipient's Catalog No.
NASA TM-4057		

4. Title and Subtitle	5. Report Date
Flight-Management Strategies for Escape From Microburst Encounters	August 1988
	6. Performing Organization Code
7. Author(s)	8. Performing Organization Report No.
David A. Hinton	L-16448
	10. Work Unit No.
9. Performing Organization Name and Address	505-66-41-55
NASA Langley Research Center Hampton, VA 23665-5225	11. Contract or Grant No.
	13. Type of Report and Period Covered
12. Sponsoring Agency Name and Address	Technical Memorandum
National Aeronautics and Space Administration Washington, DC 20546-0001	14. Sponsoring Agency Code

15. Supplementary Notes

This research represents a portion of the work performed for the author's Master of Science degree from the George Washington University.

16. Abstract

An effort is in progress by NASA, the FAA, and industry to reduce the threat of convective microburst wind-shear phenomena to aircraft. The goal of this study was to develop and test a candidate set of strategies for recovery from inadvertent microburst encounters during takeoff. Candidate strategies were developed and evaluated using a fast-time simulation consisting of a simple point-mass performance model of a transport airplane and an analytical microburst model. The results indicate that the recovery strategy characteristics that best utilize available airplane energy include an initial reduction in pitch attitude to reduce the climb rate, followed by an increase in pitch up to the stick-shaker angle of attack. The stick-shaker angle of attack should be reached just as the airplane is exiting the microburst. The shallowest angle of climb necessary for obstacle clearance should be used. If the altitude is higher than necessary, an intentional descent to reduce the airspeed deceleration should be used. Of the strategies tested, two strategies based on flight-path angle had the highest recovery altitudes and the least sensitivity to variations in the encounter scenarios.

17. Key Words (Suggested by Authors(s))	18. Distribution Statement
Wind shear Microburst Guidance Piloting techniques Air transport safety Aircraft performance	Unclassified—Unlimited Subject Category 08

19. Security Classif.(of this report)	20. Security Classif.(of this page)	21. No. of Pages	22. Price
Unclassified	Unclassified	29	A03

NASA-Langley, 1988

For sale by the National Technical Information Service, Springfield, Virginia 22161-2171